New Phytologist

Research

A lateral organ boundaries domain transcription factor acts downstream of the auxin response factor 2 to control nodulation and root architecture in *Medicago truncatula*

Cristina Kirolinko[1], Karen Hobecker[1], Marianela Cueva[1], Florencia Botto[1], Aurélie Christ[2], Andreas Niebel[3], Federico Ariel[4], Flavio Antonio Blanco[1], Martín Crespi[2] and María Eugenia Zanetti[1]

[1]Instituto de Biotecnología y Biología Molecular, Facultad de Ciencias Exactas, Universidad Nacional de La Plata, Centro Científico y Tecnológico-La Plata, Consejo Nacional de Investigaciones Científicas y Técnicas, 1900, La Plata, Argentina; [2]Institute of Plant Sciences Paris-Saclay (IPS2), CNRS, INRA, Universities Paris-Sud, Evry and Paris-Diderot, Sorbonne Paris-Cite, University of Paris-Saclay, Batiment 630, 91405, Orsay, France; [3]Laboratoire des Interactions Plantes-Microorganismes, Université de Toulouse, INRAE, CNRS, 31326, Castanet-Tolosan, France; [4]Instituto de Agrobiotecnología del Litoral, Universidad Nacional del Litoral, 3000, Santa Fe, Argentina

Author for correspondence:
María Eugenia Zanetti
Email: ezanetti@biol.unlp.edu.ar

Received: *20 December 2023*
Accepted: *21 March 2024*

New Phytologist (2024)
doi: 10.1111/nph.19766

Key words: lateral organs boundaries domain (LBD), *Medicago truncatula*, microRNA390, Nod Factor, nodulation, root architecture, symbiosis.

Summary

- Legume plants develop two types of root postembryonic organs, lateral roots and symbiotic nodules, using shared regulatory components. The module composed by the microRNA390, the *Trans-Acting SIRNA3* (*TAS3*) RNA and the Auxin Response Factors (ARF)2, ARF3, and ARF4 (miR390/*TAS3*/*ARFs*) mediates the control of both lateral roots and symbiotic nodules in legumes.
- Here, a transcriptomic approach identified a member of the Lateral Organ Boundaries Domain (LBD) family of transcription factors in *Medicago truncatula*, designated *MtLBD17/29a*, which is regulated by the miR390/*TAS3*/*ARFs* module. ChIP-PCR experiments evidenced that MtARF2 binds to an Auxin Response Element present in the *MtLBD17/29a* promoter. *MtLBD17/29a* is expressed in root meristems, lateral root primordia, and noninfected cells of symbiotic nodules.
- Knockdown of *MtLBD17/29a* reduced the length of primary and lateral roots and enhanced lateral root formation, whereas overexpression of *MtLBD17/29a* produced the opposite phenotype. Interestingly, both knockdown and overexpression of *MtLBD17/29a* reduced nodule number and infection events and impaired the induction of the symbiotic genes *Nodulation Signaling Pathway* (NSP) *1* and *2*.
- Our results demonstrate that *MtLBD17/29a* is regulated by the miR390/*TAS3*/*ARFs* module and a direct target of MtARF2, revealing a new lateral root regulatory hub recruited by legumes to act in the root nodule symbiotic program.

Introduction

LATERAL ORGAN BOUNDARIES DOMAIN (LBD) proteins are plant specific transcription factors that play essential roles in the development of lateral organs in shoots and roots (Majer & Hochholdinger, 2011; Xu *et al.*, 2016), but also in plant regeneration (Fan *et al.*, 2012), pollen development (Oh *et al.*, 2010; Kim *et al.*, 2015), photomorphogenesis (Mangeon *et al.*, 2011), ROS mediated radial growth (Dang *et al.*, 2023), the interaction with pathogenic fungi (Thatcher *et al.*, 2012), bacteria (Hu *et al.*, 2014) and nematodes (Cabrera *et al.*, 2014), as well as during the symbiotic interaction with nitrogen-fixing bacteria known as rhizobia (Schiessl *et al.*, 2019; Soyano *et al.*, 2019). LBDs are characterized by an N-terminal LATERAL ORGAN BOUNDARIES (LOB) domain consisting of a zinc finger-like motif required for DNA-binding, a Gly-Ala-Ser (GAS) block, and a leucine-zipper-like coiled-coil motif that participates in homo and hetero dimerization of this family of transcription factors (Shuai *et al.*, 2002). LBDs have been shown to interact with other transcription factors to mediate transcriptional control of their target genes, for example AtLBD18 interacts with the auxin response factors AtARF7 and AtARF19 to enhance transcription of *AtARF7* promoting lateral root development (Pandey *et al.*, 2018), whereas AtLBD6/AS2 interacts with the MYB domain protein ASYMMETRIC LEAVES1 (AS1) to mediate the repression of a *KNOX* locus controlling stem cell activity and meristem identity in Arabidopsis (Guo *et al.*, 2008).

Phylogenetic analysis classified the LBD family into two major classes, class I and class II, characterized by the presence and absence of a functional leucine-zipper-like coiled-coil motif, respectively (Majer & Hochholdinger, 2011). Most LBDs belong to class I, which was further classified into subclasses IA1, IA2,

IB, IC1/D, and IE. Members of the subclass IB were mainly implicated in the development of underground organs and/or the auxin signaling and response (Majer & Hochholdinger, 2011; Xu *et al.*, 2016; Zhang *et al.*, 2020). *AtLBD16* and *AtLBD29* are direct targets of the AtARF7 and AtARF19 transcription factors, which act as positive regulators of lateral root formation. Overexpression of *AtLBD16* and *AtLBD29* in the *arf7/arf19* double mutant background was sufficient to promote lateral root formation, rescuing the impaired lateral root formation phenotype of *arf7/arf19*, whereas dominant repression of *AtLBD16* inhibits lateral root formation (Okushima *et al.*, 2007). *AtLBD18* also acts directly or indirectly downstream of AtARF7 and AtARF19 promoting lateral root formation. Single loss of function mutants of *AtLBD16* or *AtLBD18* exhibited a significant reduction in the number of emerged lateral roots, whereas *lbd16/lbd18* double mutants showed an additive phenotype, indicating that these two LBD members act via independent molecular pathways (Lee *et al.*, 2009). More recently, an LBD member phylogenetically related to Arabidopsis AtLBD17 and AtLBD29, named SHOOTBORNE ROOTLESS (SBRL), has been shown to play an essential function in the development of lateral and shoot-borne roots in tomato (*Solanum lycopersicum*) (Omary *et al.*, 2022). Expression and function of *SBRL* orthologs during lateral root formation seem to be conserved in multiple angiosperms (Omary *et al.*, 2022). In the model legume *Medicago truncatula*, it was shown that the expression of *MtLBD1* is directly repressed by the HD-Zip transcription factor MtHB1 in specific cell types during lateral root development (F. Ariel *et al.*, 2010). Constitutive expression of *MtLBD1* resulted in a lower density of lateral roots and a longer main root, globally altering the root system architecture (F. D. Ariel *et al.*, 2010). Another member of the Class IB of LBD transcription factor, referred to as *MtLBD16* in *M. truncatula* and *ASL18/LjLBD16a* in *Lotus japonicus*, has been shown to play an essential role in lateral root development and the formation of root nodules, lateral organs formed in legume plants during the symbiotic interaction with nitrogen-fixing bacteria (Schiessl *et al.*, 2019; Soyano *et al.*, 2019). Thus, it has been proposed that legume plants have hijacked this regulator of lateral root development across species to coordinate the organogenesis of symbiotic nodules during their interaction with rhizobia (Bishopp & Bennett, 2019; Schiessl *et al.*, 2019; Soyano *et al.*, 2019, 2021).

The formation of symbiotic nodules requires the activation and coordination of bacterial infection with nodule organogenesis. The most sophisticated mechanism of infection is initiated by the attachment of the bacteria to the growing root hairs. Perception of Nod Factors released by the bacteria triggers the curling of the root hair, which entraps the bacteria, forming an infection pocket. Subsequently, the inward growth of the root hair produces a tubular structure called infection thread that progresses and ramifies to invade the dividing cortical cells (Roy *et al.*, 2020; Jhu & Oldroyd, 2023). Nodule organogenesis is initiated by the activation of cell divisions in the inner root cell layers that form the nodule primordia (Xiao *et al.*, 2014). The ontogeny of symbiotic nodules exhibits similarities and differences with lateral root development. Both developmental programs involve activation of cell division in the pericycle, endodermis, and cortex as a function of local auxin maxima (Moreno-Risueno *et al.*, 2010). However, lateral roots form from founder cells primed by periodic auxin maxima oscillation. By contrast, auxin maxima during nodule initiation is the result of a combination of the inhibition of auxin transport below the site of bacterial infection, which requires the perception of cytokinins by the CRE1 cytokinin receptor (Ng *et al.*, 2015), and the localized *de novo* biosynthesis of auxins mediated by *YUCCA* genes (Schiessl *et al.*, 2019). The shared regulatory component *LBD16* is required for both lateral root formation and nodule organogenesis. However, its expression is activated by auxin in early lateral root primordia derived from the pericycle, whereas during the root nodule symbiosis *LBD16* is activated in epidermal cells and nodule primordia by the master transcriptional regulator Nodule Inception (NIN), where, together with the nuclear factor Y subunits NF-YA1 and NF-YB, promotes nodule development (Schiessl *et al.*, 2019; Soyano *et al.*, 2019). Additional common regulatory components of lateral root and nodule formation include members of the Auxin Response Factor (ARF) family of transcription factors and products of the auxin biosynthetic genes belonging to the YUCCA family (Breakspear *et al.*, 2014; Schiessl *et al.*, 2019; Kirolinko *et al.*, 2021).

The microRNA390/*Trans Acting SIRNA3/ARF* (miR390/*TAS3/ARF*) is an evolutionarily conserved module that mediates different aspects of plant development. The miR390 guides ARGONAUTE 7 (AGO7)-mediated endonucleolytic cleavage of the *TAS3* transcript, triggering the production of secondary *trans*-acting small interference RNAs (tasiRNAs), which bound to AGO1 guide endonucleolytic cleavage of *ARF2*, *ARF3* and *ARF4* mRNAs (Xia *et al.*, 2017). We have previously shown that the miR390/*TAS3/ARF* module mediates the control of lateral root formation and root nodule symbiosis (Hobecker *et al.*, 2017; Kirolinko *et al.*, 2021; Castaingts *et al.*, 2022). Activation of the miR390/*TAS3/ARF* module by overexpression of miR390 in *M. truncatula* roots altered root architecture and impaired nodule formation and infection by *Sinorhizobium meliloti*, whereas inactivation of this module by expression of a target mimicry of miR390 or mutations in *AGO7* promotes nodule organogenesis and bacterial infection (Hobecker *et al.*, 2017). Simultaneous knockdown of *MtARF2*, *MtARF3*, and *MtARF4* or a loss of function mutation in *MtARF4a* enhances lateral root density, but negatively impacts on the elongation of lateral roots. Moreover, roots silenced in *MtARF2*, *MtARF3*, and *MtARF4* or *arf4* mutant plants are compromised in nodule organogenesis, bacterial infection, and the induction of the key symbiotic marker *Nodulation Signaling Pathway 2* (*MtNSP2*) (Kirolinko *et al.*, 2021). Here, an RNA-Seq approach identified a transcript encoding a *M. truncatula* class IB LBD member, designated *MtLBD17/29a*, as a novel target of the miR390/*TAS3/ARF* module. *MtLBD17/29a* was upregulated in *M. truncatula* roots by *S. meliloti*, but not in roots overexpressing miR390 or silenced in *MtARF2*, *MtARF3* and *MtARF4a/b*. A ChIP-PCR assay demonstrated that MtARF2 directly binds to the *MtLBD17/29a* promoter. Reverse genetic approaches indicated that *MtLBD17/29a* functions promoting the elongation of primary and lateral roots

but impairing lateral root initiation. During the root nodule symbiosis, *MtLBD17/29a* is required for nodule development and the formation of infection threads, as well as the induction of the symbiotic marker genes *MtNSP1* and *MtNSP2*. Hence, MtLBD17/29a defines a new component of the miR390/*TAS3*/*ARF* regulatory network controlling symbiotic interactions in legumes.

Materials and Methods

Biological material

Wild-type (WT) *Medicago truncatula* Jemalong A17 seeds were obtained from INRA Montpellier, France (http://www.montpellier.inra.fr). *nin-1*, *nf-ya1*, and *ern1* mutants have been described previously (Marsh *et al.*, 2007; Middleton *et al.*, 2007; Laporte *et al.*, 2014). *Sinorhizobium meliloti* strain 1021 (Meade & Signer, 1977) or the same strain expressing RFP (Tian *et al.*, 2012) were used for root inoculation. *Agrobacterium rhizogenes* strain Arqua1 used for hairy root transformations was previously described (Quandt *et al.*, 1993).

Constructs for plant transformation

The *pLBD17/29a-gfp-gus* construct was generated by amplifying the 1460-bp region upstream of the translational initiation codon of *MtLBD17/29a* using pLBD17/29a F and pLBD17/29a R primers (Supporting Information Table S1) and *pfu* DNA polymerase (Promega). The resulting DNA fragment was cloned into the pENTR/D-TOPO vector (Thermo Fisher Scientific, Waltham, MA, USA) and then recombined into the Gateway-compatible binary vector pKGWFS7,0 (Karimi *et al.*, 2002) using LR Clonase according to manufacturer's instructions (Thermo Fisher Scientific). *LBD17/29a* RNAi 1 and *LBD17/29a* RNAi 2 constructs were generated by PCR amplification using cDNA from *M. truncatula* roots as template, *LBD17/29a* RNAi 1 F, *LBD17/29a* RNAi 1 R, *LBD17/29a* RNAi 2 F and *LBD17/29a* RNAi 2 R primers (Table S1) and *pfu* DNA polymerase. The amplified fragments were cloned into the pENTR/D-TOPO vector and then recombined into the destination vector pK7GWIWG2D (II) (Karimi *et al.*, 2007) to generate the *LBD17/29a* RNAi 1 and *LBD17/29a* RNAi 2 constructs. The *GUS* RNAi construct was previously described (Kirolinko *et al.*, 2021). The OXLBD17/29a construct was generated by PCR amplification using *M. truncatula* cDNA as template, OXLBD17/29a F and OXLBD17/29a R primers (Table S1) and *pfu* DNA polymerase. The amplified fragment was cloned into the pENTR/D-TOPO vector and then recombined into the Gateway-compatible binary vector pK7WG2D,1 (Karimi *et al.*, 2002). The pK7GWIWG2D (II) and pK7WG2D,1 vectors contain the *rolD*:*GFP* transcriptional unit for the detection and selection of transgenic roots; therefore, only roots with detectable GFP fluorescence (> 80% of roots) were considered for expression and phenotypic analyses. ARF2 open reading frame was amplified from cDNA using HF-ARF2 R and HF-ARF2 F primers (Table S1), cloned into the pENTRY/D-TOPO vector and then recombined into the p35S:HF-GAT vector (Mustroph *et al.*, 2010). All constructs were verified by sequencing and introduced into *A. rhizogenes* Arqua1 (Quandt *et al.*, 1993) by electroporation.

Growth of *M. truncatula*, hairy root transformation, inoculation with rhizobia and NF treatment

Seeds were surface-sterilized and germinated as previously described (Hobecker *et al.*, 2017). Transgenic roots were generated by *A. rhizogenes*-mediated transformation essentially as described previously (Boisson-Dernier *et al.*, 2001) and transferred to Petri dishes containing Fahraeus agar media (Fahraeus, 1957) supplemented with 8 mM KNO_3 and 12.5 μg ml^{-1} kanamycin for 7 d. Seedlings were grown at 25°C on a 16 h : 8 h, day : night cycle with radiation of 200 μmol m^{-2} s^{-1} under mixed illumination with four OSRAM cool daylight L36W/765 tubes per one OSRAM FLUORA L36W/77 tube. For root architecture analysis, composite plants, consisting of a nontransgenic shoot and transgenic hairy roots, were transferred to slanted boxes containing Fahraeus media supplemented or not with 8 mM KNO_3 and grown under the conditions described above for 15 d. For inoculation with rhizobia, plants that developed hairy roots were transferred to slant boxes containing Fahraeus media free of nitrogen covered with sterile filter paper. Seven days after transplantation, roots were inoculated with 10 ml of a 1 : 1000 dilution of *S. meliloti* 1021 (Meade & Signer, 1977) or with the same strain expressing RFP grown in liquid TY media until OD_{600} reached 0.8, or with 10 ml of water as control (mock treatment). For Nod Factor treatment, WT, *nf-ya1*, *ern1* and *nin* mutants were grown on slant boxes containing Fahraeus media free of nitrogen for 7 d and then treated with 10 ml of a suspension of 10^{-8} M of *S. meliloti* purified NFs or with 10 ml of water as a mock treatment.

RNA extraction and RT-qPCR

Total RNA extraction and cDNA synthesis were performed as previously described (Hobecker *et al.*, 2017). Expression analysis was performed by reverse transcription quantitative polymerase chain reaction as previously described (Reynoso *et al.*, 2013) using gene specific primers listed in Table S1. Expression levels were normalized to *HIS3L*, which was validated using GNORM software (Vandesompele *et al.*, 2002), as previously reported by F. Ariel *et al.* (2010) and Reynoso *et al.* (2013). Statistical significance between samples was determined by an unpaired two-tailed Student's *t*-test.

RNA-Seq library preparation and sequencing

RNA was extracted from OX390 and EV roots at 48 hpi with *S. meliloti* 1021 or with water (mock) as previously described (Hobecker *et al.*, 2017). Two biological replicates were obtained with a minimum of 30 transgenic roots per condition. RNA integrity and concentration was analyzed by capillary electrophoresis using a Bioanalyzer 2100 (Agilent Technologies, Santa Clara, CA, USA). Libraries were prepared from 1.5 μg of RNA

using the TruSeq RNA Illumina Sample Preparation Kit v.2 and sequenced at the Université de Paris Saclay, France using the HiSeq4000 platform with single end reads of 76 nts.

Data analysis

RNA-Seq reads were aligned to the *M. truncatula* genome v.5 (Pecrix *et al.*, 2018) using HISAT2 (Kim *et al.*, 2019). Transcript assembly and quantification of full-length transcripts was performed using STRINGTIE (Pertea *et al.*, 2015). StringTie files for each sample were merged using the STRINGTIE MERGE tool. Tables of 'genes counts' were generated using STRINGTIE, and the DESEQ2 tool (Love *et al.*, 2014) was used to identify DEGs keeping only the genes that had FPKM values ≥ 1 in at least one of the libraries. Heatmap maps were generated using the Morpheus algorithm (MORPHEUS, https://software.broadinstitute.org/morpheus/).

Chromatin immunoprecipitation assay followed by quantitative polymerase chain reaction

Chromatin immunoprecipitation (ChIP) assays were performed essentially as described (Ariel *et al.*, 2020). Briefly, formaldehyde-crosslinked chromatin from HF-ARF2 roots 48 hpi with *S. meliloti* 1021 was sonicated in a Bioruptor Pico (30 s on/30 s off pulses, for 10 cycles). Fragmented chromatin was incubated with anti-FLAG or IgG bound to Protein G-coupled magnetic beads (Dynabeads, Thermo Fisher Scientific) overnight at 4°C in a rotary wheel. Sonicated chromatin was processed in parallel and considered as input. Crosslinking was reversed by incubation with Proteinase K and DNA was purified by 25 : 24 : 1 phenol : chloroform : isoamyl alcohol extraction and analyzed by quantitative polymerase chain reaction using primers listed in Table S1.

Fluorescent microscopy

GFP fluorescence in roots was visualized and photographed with an inverted microscope (Olympus IX51, Olympus Corporation, Shinjuku City, Tokyo, Japan) using UV light with appropriate filters for GFP. GFP fluorescence in RFP-expressing *S. meliloti* inoculated roots and nodules was detected by confocal microscopy using an SP5 inverted confocal microscope (Leica Microsystems, Wetzlar, Germany). GFP and RFP were excited with 488- and 543-nm lasers, and emissions were collected from 498 to 552 nm and from 578 to 626 nm, respectively. Images were processed using the LAS IMAGE ANALYSIS software (Leica Microsystems).

GUS staining

Histochemical GUS staining was performed as previously described (Hobecker *et al.*, 2017). Cross sections (70 μm) of roots were obtained from samples embedded in 6% agarose using a vibratome Leica VT1000 S. GUS-stained tissue was visualized and photographed under white light using an inverted microscope (Olympus IX51).

Phenotypic analyses

For root architecture analysis, composite plants were transferred to slant boxes containing agar-Fahraeus medium supplemented or not with 8 mM KNO_3. Each root emerged directly from the sectioned radicle inoculated with *A. rhizogenes* was considered a primary root in the hairy root system, whereas roots emerged from primary roots were considered lateral roots. The number of lateral roots per centimeter of primary root, the length of primary and lateral roots, and the length of the aerial part were determined 15 d after transplanting. For nodulation analysis, composite plants were transferred to slant boxes containing nitrogen-free Fahraeus medium and, 7 d after transplantation, inoculated with *S. meliloti* 1021. The number of nodules was recorded at different times after inoculation as described previously (Hobecker *et al.*, 2017). Nodules were classified as pink (nitrogen-fixing mature nodules) or white (immature nodules) according to Traubenik *et al.* (2020). Live/dead assay of bacterial cells using SYTO9/Propidium iodine staining was essentially performed as previously described (Traubenik *et al.*, 2020). For determination of shoot and root dry weight, the aerial tissue or the whole root system was collected at 21 dpi with *S. meliloti*, dried at 80°C for 24 h and weighted using an analytical balance. Three independent biological replicates were performed. For analysis of infection events, 7 d after transplantation, roots were inoculated with the RFP-expressing *S. meliloti* strain and 7 dpi infection events were visualized, quantified, and imaged in an Olympus IX51 inverted microscope. Infection events were classified as microcolonies, ITs terminating in the root hair, ITs reaching the base of the epidermal root hair or ITs that reached and ramified in the cortical cells as previously described (Kirolinko *et al.*, 2021). In all cases, three independent biological replicates were performed with at least 10 independent roots per replicate analyzed.

Results

Overexpression of miR390 altered the transcript levels of hundreds of genes normally induced in response to rhizobia

To identify novel putative targets of the miR390/*TAS3*/*ARF* module that may play a role in the root nodule symbiosis, an RNA-Sequencing (RNA-Seq) approach was applied on miR390-overexpressing roots (OX390) and on roots transformed with the empty vector (EV) at 48 h postinoculation with water (mock) or with *S. meliloti* (Sm) (Fig. 1a). Overexpression of miR390 was verified on both biological replicates used for Illumina RNA-Seq (Fig. 1b,c). On average, 25 million reads per library were obtained, and nearly 90% of the reads mapped to the *M. truncatula* A17 r5.0 (MtruncA17r5.0-ANR) genome version (Table S2). Pearson correlation analysis verified the high reproducibility between biological replicates for all samples (Fig. S1). *In silico* analysis using HISAT2, STRINGTIE, and DESEQ2 identified 1486 and 1345 differentially expressed genes (DEGs) in response to *S. meliloti* in EV and OX390 roots, respectively (Fig. 1c; Tables S3–S7). Most of the well-known symbiotic genes, such as *MtENOD11*, *MtNIN*, *MtNPL*, *MtNF-YA1*, and *MtNF-YA2*, were included in shared upregulated DEGs (Fig. 1d;

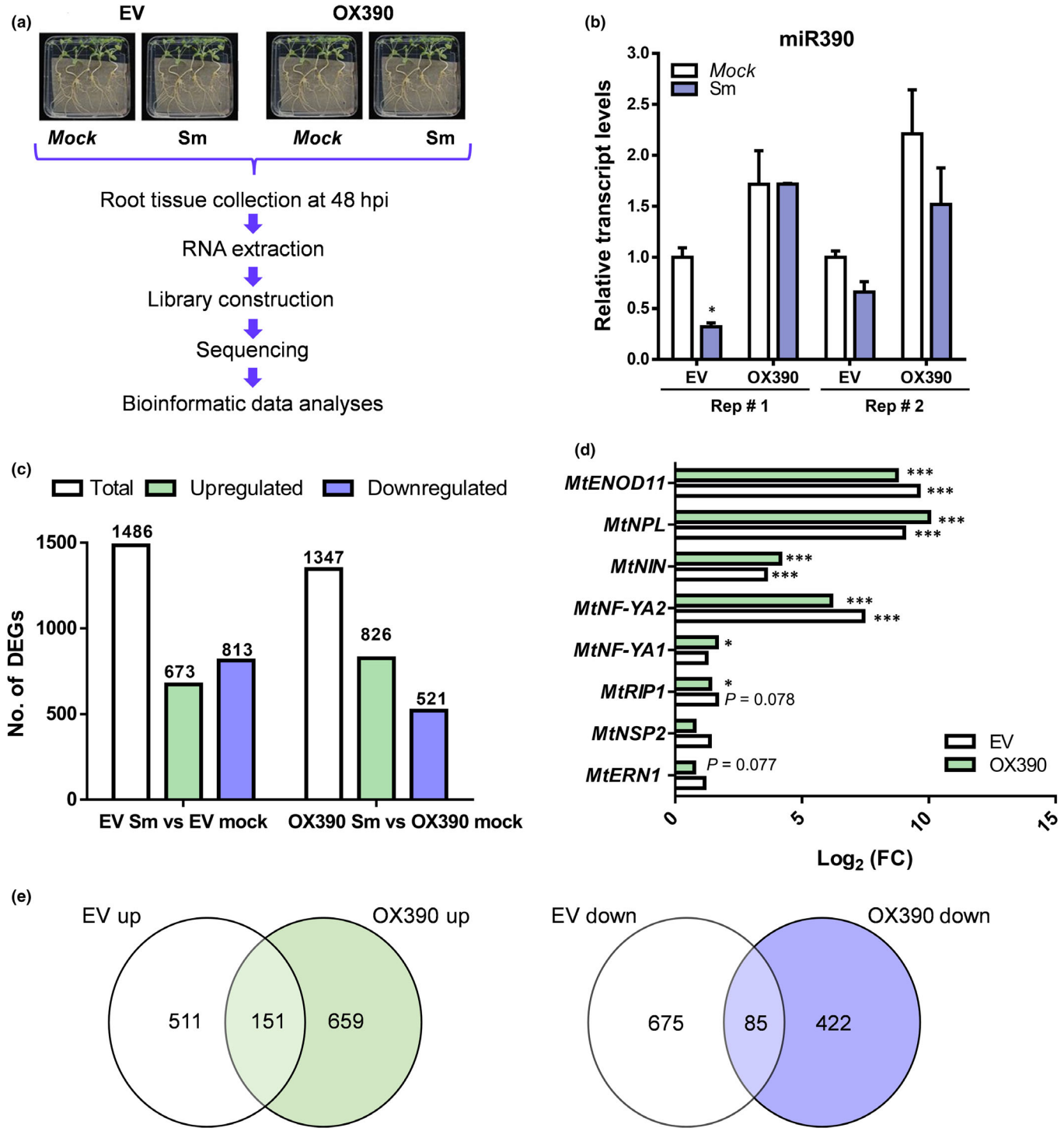

Fig. 1 Transcriptomic analysis of miR390 overexpressing roots under symbiotic and nonsymbiotic conditions. (a) Schematic overview of the experimental design. Roots transformed with the empty vector (EV) or with a construct for overexpression of miR390 (OX390) were inoculated with water (mock) or with *Sinorhizobium meliloti* (Sm). After 48 hpi, the whole root extracts were collected and subjected to total RNA extraction followed by RNA-Seq to characterize changes in the transcriptome. Two independent biological replicates were obtained using root tissues from > 20 plants per experiment and condition. (b) Reverse transcription quantitative polymerase chain reaction validation analysis of miR390 overexpression. RNA was extracted from EV and OX390 roots, and expression levels were determined by reverse transcription quantitative polymerase chain reaction, normalized to *HIS3L*, and expressed relative to the EV mock sample. Each bar represents the mean ± SE of two biological replicates. Asterisks indicate statistically significant differences with a *P*-value ≤ 0.05 in an unpaired two-tailed Student's *t*-test. (c) Number of genes differentially regulated in EV Sm vs EV mock and OX390 Sm vs OX390 mock samples ($1 < Log_2FC < -1$, $P \leq 0.05$ as identified by DESeq2). (d) Fold change (FC) of the expression levels of early symbiotic marker genes in response to rhizobia inoculation. Asterisks indicate statistically significant differences (*, $P \leq 0.05$; ***, $P \leq 0.001$) according to DESeq2 parameters. (e) Venn diagrams comparing up- and downregulated differentially expressed genes (DEGs) in response to rhizobia in EV and OX390 roots.

Table S8). However, the overlap between rhizobia regulated DEGs in EV and OX390 roots was very limited, representing only 11.4% and 7.2% of the up and downregulated DEGs, respectively (Fig. 1e). Our transcriptomic approach highlighted the strong influence of the miR390/*TAS3*/*ARF* module on the early symbiotic response.

Induction of *MtLBD17/29a* in response to rhizobia is impaired by activation of the miR390/*TAS3* pathway or simultaneous silencing of *MtARF2*, *MtARF3* and *MtARF4*

Functional classification using Gene Ontology (GO) revealed that one of the most prominent categories among DEGs is transcriptional regulation (Fig. S2; Table S9), including numerous members of the AP2/ERF, MYB, C2H2, GRAS, and WRKY families of transcription factors (Fig. 2a). Two members of the LBD family with Gene IDs *MtrunA17Chr1g0184271* and *MtrunA17Chr5g0402611* were induced in response to rhizobia in EV but not in OX390 roots. Moreover, *MtrunA17Chr1g0184271* was slightly downregulated in OX390 roots (Fig. 2a). A phylogenetic analysis of *M. truncatula* and Arabidopsis LBD members indicated that the protein encoded by *MtrunA17Chr1g0184271* belongs to the class IB and is closely related to AtLBD17 and AtLBD29. Within the subclade containing the product of *MtrunA17Chr1g0184271*, there was also the product of *MtrunA17Chr7g0261031* (Fig. S3). A syntenic analysis did not resolve which *M. truncatula* member could be the syntenic gene of *AtLBD17* and *AtLBD29* (Fig. S4); thus, we designated *MtrunA17Chr1g0184271* and *MtrunA17Chr7g0261031* as *MtLBD17/29a* and *MtLBD17/29b*, respectively. *MtLBD17/29b* mRNA levels did not significantly change either in response to rhizobia inoculation or by overexpression of miR390 (Table S3). Since Class IB LBD members have been implicated in auxin-mediated development of lateral root organs in different plant species (Okushima *et al.*, 2007; F. Ariel *et al.*, 2010; F. D. Ariel *et al.*, 2010; Schiessl *et al.*, 2019) and *AtLBD16*, *AtLBD18*, and *AtLBD29* have been shown to act downstream of ARF7/ARF19 to control lateral root formation (Okushima *et al.*, 2007; Zhang *et al.*, 2020), we focused our analysis on *MtLBD17/29a*. Reverse transcription quantitative polymerase chain reaction experiments verified that *MtLBD17/29a* mRNA levels accumulated to significantly higher levels in response to rhizobia in EV roots, but not in OX390 or roots silenced in *MtARF2*, *MtARF3* and *MtARF4a/b* (*ARF2/3/4* RNAi) (Fig. 2b). By contrast, roots of the *ago7-3* mutant, where levels of *MtARF2*, *MtARF3*, and *MtARF4* are uncoupled from the miR390/*TAS3* module, showed higher up-regulation of *MtLBD17/29a* mRNA levels upon rhizobia inoculation as compared with WT roots (Fig. 2b). These results suggest that the expression of *MtLBD17/29a* is controlled by the miR390/*TAS3*/*ARF* pathway during the establishment of root nodule symbiosis.

MtLBD17/29a is a direct target of MtARF2

A search of Auxin Response Elements (AREs) in the promoter sequences of *MtLBD17/29a* identified two putative AREs, named ARE1 and ARE2, in the 2 kb region upstream of the transcriptional start site of *MtLBD17/29a* (Fig. 2c), suggesting that *MtLBD17/29a* may be directly regulated by ARF transcription factors. On the contrary, no ARE elements were found in the 2 kb region upstream of the transcriptional start site of its closest homolog *MtLBD17/29b*, indicating that there are no proximal ARF target sites in this promoter. We also searched for ARE motifs in the promoter sequences of *MtNSP2*, which was proposed as a putative target of the ARF family (Hobecker *et al.*, 2017; Kirolinko *et al.*, 2021), as well as in the promotor region of *MtARF2*, *MtARF3*, *MtARF4a* and *MtARF4b*, since ARF members has been shown to participate in a positive feedback transcriptional regulatory mechanism (Pandey *et al.*, 2018). Two AREs were found in the promoter region of *MtNSP2*, one in the promoter regions of *MtARF3*, *MtARF4a* and *MtARF4b* and no AREs were found in the promoter of *MtARF2* (Fig. 2c). To assess whether these genes were direct targets of ARF transcription factors, we performed Chromatin Immunoprecipitation assays followed by quantitative polymerase chain reaction (ChIP-qPCR). ChIP assays were conducted on chromatin obtained from *S. meliloti* inoculated roots that constitutively expressed a FLAG tagged version of MtARF2 (FLAG-ARF2), using a commercial α-FLAG antibody or α-IgGs as a negative control. The expression of FLAG-ARF2 was confirmed in FLAG-ARF2 roots by reverse transcription quantitative polymerase chain reaction using transgene specific primers (Fig. S5a). Reverse transcription quantitative polymerase chain reaction using primers that detect both the endogenous *MtARF2* and the transgene *FLAG-ARF2* revealed an increase of 20-fold in *MtARF2* mRNA levels in FLAG-ARF2 roots as compared to EV roots, and a concomitant increase of eight-fold in *MtLBD17/29a* mRNA levels (Fig. S5b). The increase in *MtARF2* levels did not significantly alter nodule formation or infection, indicating that other components of the module are required to promote the root nodule symbiosis (Fig. S5c, d). After ChIP, quantitative polymerase chain reactions were conducted using specific primers that flanked each ARE motif in the *MtARF4a*, *MtARF4b*, *MtARF3*, *MtNSP2* and *MtLBD17/29a* promoters. The ARE1 motif of *MtLBD17/29a* promoter was enriched by > 13-fold in the genomic DNA fragments immunoprecipitated with α-FLAG antibody, whereas the ARE2 motif present in the *MtNSP2* promoter was enriched by twofold in the immunoprecipitated with α--FLAG as compared to the samples immunoprecipitated with IgG (Fig. 2d), indicating that both *MtLBD17/29a* and the symbiotic gene *MtNPS2* are direct targets of MtARF2. Quantitative polymerase chain reaction with specific primers for *ACTIN11* used as a negative control did not reveal any enrichment. ChIP-qPCR also showed an enrichment of two-fold for the ARE motif present in the *MtARF4a* promoter, but not for those ARE present in the promoters of *MtARF3* and *MtARF4b*, indicating that MtARF2 can directly modulate the expression of *MtARF4a* (Fig. 2d). In conclusion, our ChIP analysis indicated that the MtARF2 binds with high affinity to the *MtLBD17/29a* promoter.

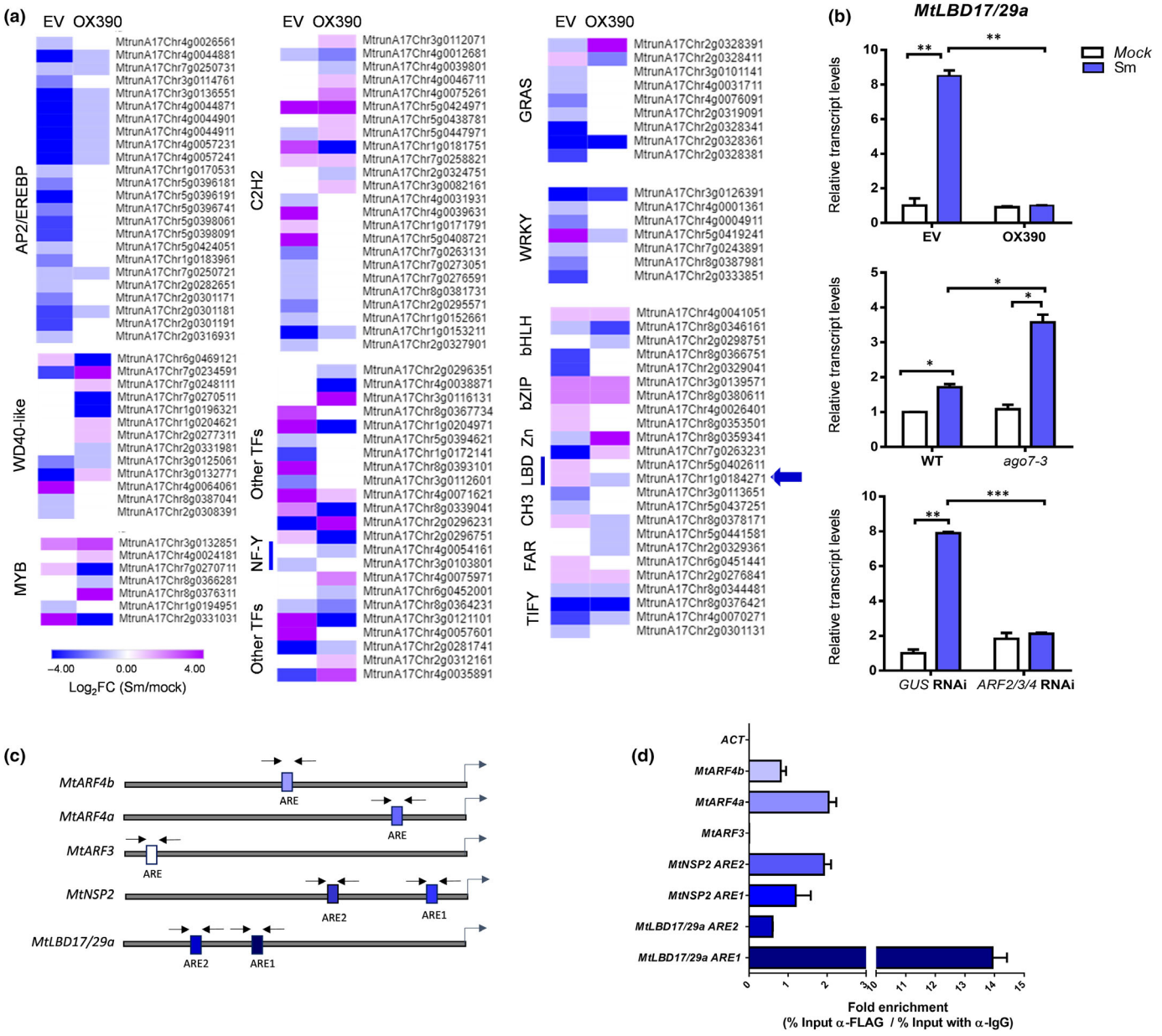

Fig. 2 *MtLBD17/29a* is a target of the miR390/*TAS3*/*ARFs* module. (a) Heat maps showing $\log_2$ fold change (FC) of mRNAs encoding transcription factors from different families in *Sinorhizobium meliloti* (Sm) inoculated vs water inoculated (mock) empty vector (EV) and OX390 roots. Heat maps and hierarchical clustering analyses were performed using Morpheus. The purple arrow points to the *MtLBD17/29a* (*MtrunA17Chr1g0184271*) transcript. (b) Transcript levels of *MtLBD17/29a* in EV, OX390, *GUS* RNAi, and *ARF2/3/4* RNAi transgenic roots, as well as in root tissues of wild-type (WT) and *ago7-3* mutant plants, inoculated with *S. meliloti* (Sm, purple bars) or water (mock, white bars) for 48 h. Expression levels were determined by reverse transcription quantitative polymerase chain reaction and normalized to the levels of the *MtHIS3L* transcript. Values are expressed relative to the WT, *GUS* RNAi, or EV mock-treated sample, which was set at 1. Bars are SEM of three biological replicates. Asterisks indicate statistically significant differences (*, $P \leq 0.05$; **, $P \leq 0.01$; ***, $P \leq 0.001$) in an unpaired two-tailed Student's *t*-test. (c) Schematic representation of ARE motifs found in 2 kb sequences upstream of the Transcription Start Site (TTS) of *MtARF4a*, *MtARF4b*, *MtARF3*, *MtNSP2*, and *MtLBD17/29a*. Black arrows represent the primers used for the chromatin immunoprecipitation (ChIP)-PCR analysis. Gray arrows indicate the TSS. (d) Quantification of ChIP by quantitative polymerase chain reaction. The regions of interest were quantified by quantitative polymerase chain reaction. Fold enrichment was calculated by normalizing the percentage of the input in ChIP samples obtained using anti-FLAG to the percentage of the input in ChIP samples obtained using anti-IgGs. Bars represent the mean and SEM of two technical replicates. A fragment of the *Actin 11* (*ACT*) gene, which does not contain AREs, was used as negative control.

MtLBD17/29a is expressed in root meristems and influences root architecture

Considering that *MtARF2*, *MtARF3* and *MtARF4* modulate root architecture in *M. truncatula* (Kirolinko *et al.*, 2021) and that *MtLBD17/29a* is a direct target of MtARF2, we asked whether this member of the LBD family play a role in root development, as its counterparts in other plant species (Okushima *et al.*, 2007; Omary *et al.*, 2022). Inspection of public transcriptomic data during lateral root formation indicated that *MtLBD17/29a*

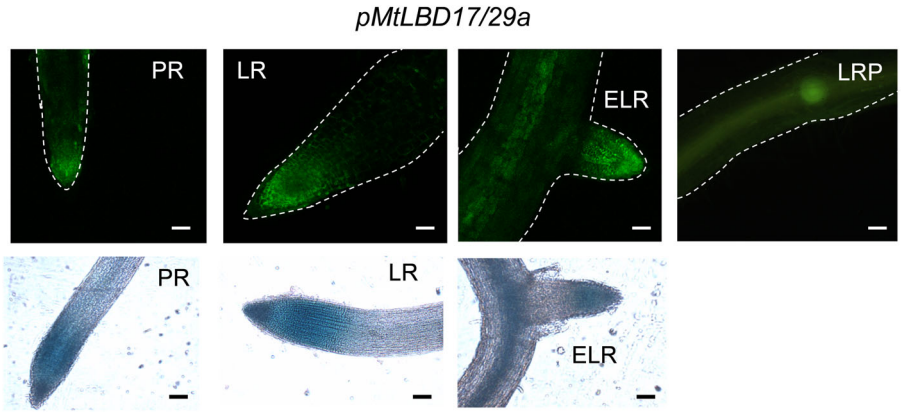

Fig. 3 Expression analysis of *MtLBD17/29a* in primary and lateral roots. Expression of the *GFP* and *GUS* reporter genes in primary and lateral roots transformed with the *pMtLBD17/29a: GFP-GUS*. Dashed lines mark the epidermal cells of roots. ELR, emerged lateral root; LR, Lateral root; LRP, lateral root primordia formed 48 h after seedling were turned 135° to induce lateral root formation; PR, primary root. Bars, 50 μm.

mRNA levels are downregulated at early stages of lateral root formation (Fig. S6), that is when pericycle cells have undergone periclinal and anticlinal cell divisions (Schiessl *et al.*, 2019). A transcriptional fusion of the *MtLBD17/29a* promoter to reporter genes (*pMtLBD17/29a: GFP-GUS*) revealed that *MtLBD17/29a* is expressed mainly in the meristems of primary and lateral roots, as well as in lateral root primordia formed 48 h after seedling were turned 135° to induce lateral root formation (Fig. 3). At this stage, multiple rounds of periclinal cell divisions formed a cone shaped lateral root primordium as reported by Schiessl *et al.* (2019). Expression of *MtLBD17//29a* in lateral root primordia agrees with the expression of *AtLBD29* and *SBRL* in Arabidopsis and tomato, respectively (Okushima *et al.*, 2007; Porco *et al.*, 2016; Omary *et al.*, 2022), suggesting that the expression of this LBD member in lateral root primordia is conserved across the plant kingdom. In addition, the expression of *MtLBD17/29a* coincides with the primary and lateral roots expression pattern of other components of the miR390/TAS3/ARF pathway such as *MtARF3* and *MtARF4a* (Kirolinko *et al.*, 2021).

To assess the role of *MtLBD17/29a* in root development, we knocked down *MtLBD17/29a* in *M. truncatula* roots using two different RNA interference (RNAi) constructs, that is one complementary to the coding region and the other complementary to the 3′ untranslated region, designated as *MtLBD17/29a* RNAi 1 and *MtLBD17/29a* RNAi 2, respectively (Fig. 4a). Both constructs significantly reduced *MtLBD17/29a* transcript levels (78% and 65% reduction for *MtLBD17/29a* RNAi 1 and *MtLBD17/29a* RNAi 2, respectively), but did not affect mRNA levels of its closest homolog *MtLBD17/29b* or of *MtLBD16* (Fig. 4b). In the absence of nitrogen, knockdown of *MtLBD17/29a* using either *MtLBD17/29a* RNAi 1 or *MtLBD17/29a* RNAi 2 resulted in a reduction of primary and lateral root length (Fig. 4c,d,h) and an increase in lateral root density (number of lateral roots per cm of primary root) when compared with *GUS* RNAi roots (Fig. 4e,h). This increase in lateral root density could not be explained by the reduction of primary root length since total number of emerged lateral roots was enhanced in *MtLBD17/29a* RNAi roots as compared with *GUS* RNAi root (Fig. 4f). The reduction in the length of primary and lateral roots also impacted on the aerial part, limiting the elongation of the shoot (Fig. 4f,g). Similar changes in root architecture and shoot elongation were observed in *MtLBD17/29a* RNAi plants when the media was supplemented with KNO_3 as a source of nitrogen (Fig. S7). On the contrary, overexpression of *MtLBD17/29a*, which caused a nearly 100-fold increase in *MtLBD17/29a* mRNA levels (Fig. 4i), enhanced the elongation of the primary and lateral roots but decreased lateral root density when plants were grown in the absence of nitrogen (Fig. 4j–l,n). This root phenotype also negatively impacted on shoot elongation (Fig. 4m,n). In the presence of nitrogen, overexpression of *MtLBD17/29a* had no impact on primary root length but enhanced lateral root length and reduced lateral root density (Fig. S8). These results suggest that *MtLBD17/29a* promotes lateral root elongation but limits lateral roots initiation and/or emergence in *M. truncatula*.

MtLBD17/29a expression in response to Nod Factor depends on *MtNIN* and is detected in noninfected cells of the nodule

MtLBD17/29a mRNA levels increased in *M. truncatula* roots at 48 hpi with *S. meliloti* (Fig. 2), thus, we wondered whether its expression was dependent on the Nod Factor signaling pathway. Levels of *MtLBD17/29a* accumulated to significantly higher levels after 48 h of Nod Factor treatment in WT roots, as well as in *ern1* and *nf-ya1* mutants, but not in a loss of function *nin* mutant as determined by reverse transcription quantitative polymerase chain reaction experiments (Fig. 5a). Inspection of publicly available RNA-Seq data of spot-inoculated roots (Schiessl *et al.*, 2019) verified that *MtLBD17/29a*, along with other members of the Class IB of LBDs, is transiently upregulated at early stages of the symbiosis in WT roots; however, up-regulation of *MtLBD17/29a* was not observed in the *nin* mutant background (Fig. S9), supporting the notion that induction of *MtLBD17/29a* in response to rhizobia is *NIN*-dependent.

pMtLBD17/29a:GFP-GUS analysis in *M. truncatula* roots at 6 d postinoculation (dpi) with an RFP-expressing *S. meliloti* strain revealed that *MtLBD17/29a* promoter activity was detected in the dividing cells below the infected root hair (Fig. 5b). In young nodules of 10 dpi, the GFP expression was observed in noninfected cells surrounding the infected cells. Later, in nodules of 21 dpi, GFP signal was detected in noninfected cells surrounding

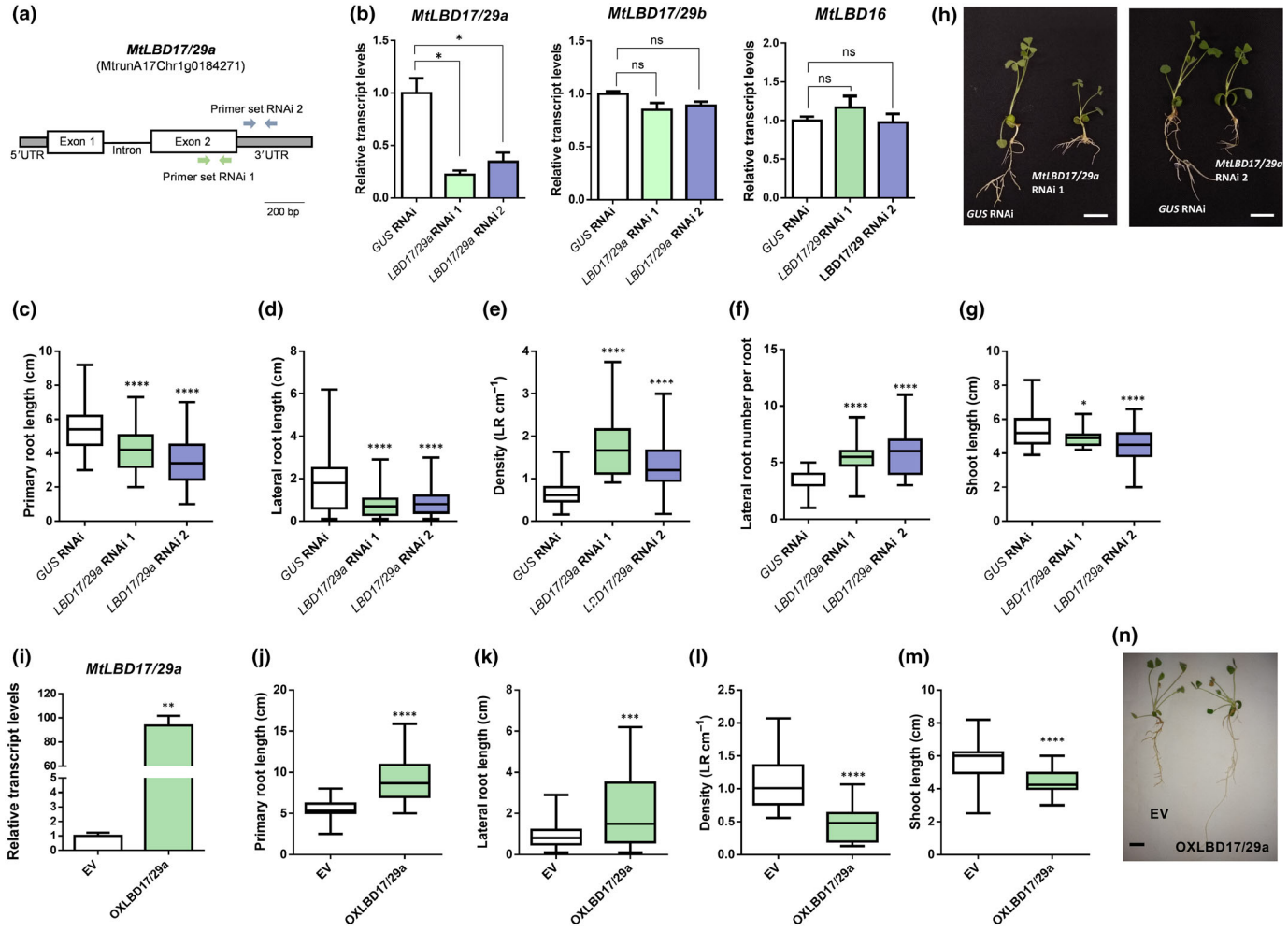

Fig. 4 Knockdown and overexpression of *MtLBD17/29a* alter root architecture. (a) Schematic representation of the *MtLBD17/29a* construct and the position of the primers used to generate the *LBD17/29a* RNAi 1 (green arrows) and *LBD17/29a* RNAi 2 (blue arrows) constructs. (b) mRNA levels of *MtLBD17/29a*, *MtLBD17/29b* and *MtLBD16* in *GUS* RNAi, *LBD17/29a* RNAi 1 and *LBD17/29a* RNAi 2 roots. Expression values were determined by reverse transcription quantitative polymerase chain reaction, normalized to *MtHIS3L*, and expressed relative to the *GUS* RNAi sample, which was set at 1. (c–g) Primary root length (c), lateral root length (d), lateral root density (e), lateral root number per plant (f) and shoot length (g) measured in *GUS* RNAi, *LBD17/29a* RNAi 1, and *LBD17/29a* RNAi 2 plants grown at 15 d after at 15 d after transplantation to square Petri dishes containing slanted agar-Fahraeus medium in the absence of nitrogen. (h) Representative pictures of *GUS* RNAi, *LBD17/29a* RNAi 1, and *LBD17/29a* RNAi 2 plants at 15 d after transplantation. (i) mRNA level of *MtLBD17/29a* in EV and OXLBD17/29a roots determined by reverse transcription quantitative polymerase chain reaction, normalized to *MtHIS3L*, and expressed relative to the empty vector (EV) sample, which was set at 1. (j–m) Primary root length (j), lateral root length (k), lateral root density (l) and shoot length (m) were measured in EV and OXLBD17/29a plants grown in the absence of nitrogen at 15 d after transplantation to square Petri dishes slanted agar-Fahraeus medium in the absence of nitrogen. In (b) and (i) each bar represents the mean ± SE of three biological replicates with at least 10 plants per replicate. Asterisks indicate statistically significant differences between *GUS* RNAi and *LBD17/29a* RNAi 1 or*LBD17/29a* RNAi 2 or between EV and OXLBD17/29a roots in an unpaired two-tailed Student's *t*-test ($P \leq 0.05$). ns, no significant. In (c–g) and (j–m) boxes extend from the 25th to 75th percentiles, the middle line is the median, and whiskers extend to the minimum and maximum values of three technical replicates with at least 25 plants each. Asterisks denote statistically significant differences between *GUS* RNAi and *LBD17/29a* RNAi 1 or *LBD17/29a* RNAi 2 plants or between EV and OXLBD17/29a plants in an unpaired two-tailed Student's *t*-test (*, $P \leq 0.05$; **, $P \leq 0.01$; ***, $P \leq 0.001$; ****, $P \leq 0.0001$). (n) Representative image of EV and OXLBD17/29a plants at 15 dag. Bars: (h, n) 1 cm.

the infected cells of the infection, transition, and nitrogen-fixing zones (Fig. 5b). This spatial expression pattern is reminiscent of that previously observed for the promoters of *MIR390b* and *MtARF4a* (Hobecker *et al.*, 2017; Kirolinko *et al.*, 2021). Since the *MtLBD17/29a* promoter is targeted by *MtARF2*, we aimed to analyze whether the spatial expression pattern of *MtLBD17/29a* overlaps with that of *MtARF2*. Since we were unable to amplify the *MtARF2* promoter after several attempts using different primers combinations and PCR conditions (Kirolinko *et al.*, 2021), we explored the expression pattern of *MtARF2* using single nuclei RNA-Seq data described by Cervantes-Perez *et al.* (2022). This analysis revealed that *MtARF2* transcripts ubiquitously accumulate in the nuclei of root cells, and increase in root hair, epidermal, cortical, and stele cells at 48 hpi with *S. meliloti* (Fig. S10). This expression pattern partially coincides with that of *MtLBD17/29a*, which is upregulated at 48 hpi but not

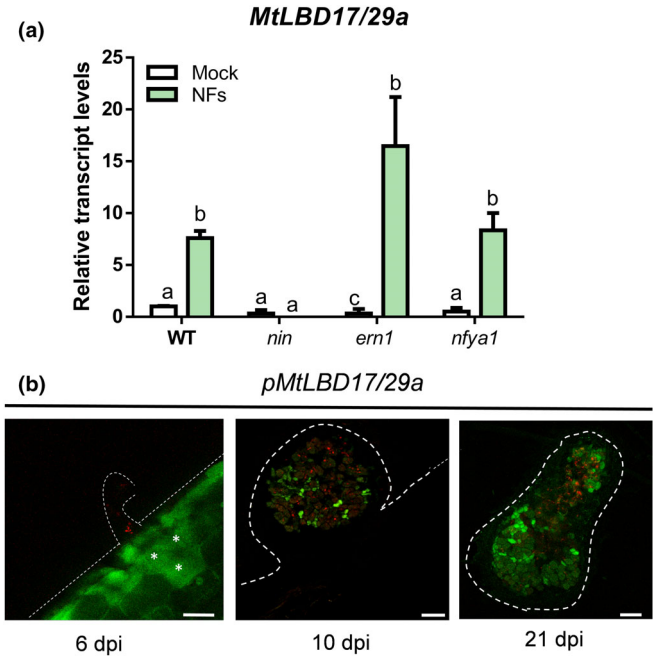

Fig. 5 *MtLBD17/29a* expression during symbiosis depends on the *MtNIN* and is detected in noninfected cells of the nodules (a) Levels of *MtLBD17/29a* were analyzed in root tissue of wild-type (WT) and *nin*, *ern1* and *nf-ya1* mutant plants treated with 10^{-8} M purified Nod Factors (NFs, green bars) or water (mock, white bars) for 48 h. Expression levels were determined by reverse transcription quantitative polymerase chain reaction and normalized to the levels of the *MtHIS3L* transcript. Values are expressed relative to the WT mock-treated sample, which was set at 1. Bars are SEM of three biological replicates. Different letters above the bars indicate statistically significant differences between samples in an unpaired two-tailed Student's *t*-test with $P \leq 0.05$. (b) *Promoter:GFP-GUS* reporter expression analysis of *MtLBD17/29a* at different stages of the symbiotic interaction with *Sinorhizobium meliloti*. GFP fluorescence was analyzed in roots transformed with the *pMtLBD17/29a:GFP-GUS* construct at 6 d postinoculation (dpi) and in developing nodules at 10 and 21 dpi with a strain of *S. meliloti* that expressed the red fluorescent protein (RFP). Dashed lines mark the epidermal cells of roots and nodules. Asterisks mark the dividing cells below the infected root hair. Bars, 50 μm.

expressed in root hair (Fig. 5b, left panel). In mature nodules, previous inspection of RNA-Seq data of nodule section described by Roux *et al.* (2014) revealed that, albeit enriched in the meristematic zone, *MtARF2* mRNA levels were detected in all differentiation zones of the nodule (Hobecker *et al.*, 2017), overlapping with the expression of *MtLBD17/29a* in the infection, transition, and fixation zones (Fig. 5b, right panel).

Altered levels of *MtLBD17/29a* impair nodule formation, infection by rhizobium, and induction of early nodulation markers

Then, we explored the function of *MtLBD17/29a* during the root nodule symbiosis. Roots silenced in *MtLBD17/29a* formed fewer nodules that were not fully developed based on the morphology of the nodules, the quantification of white and pink nodules and the expression of leghemoglobin coding gene *MtLgHb1* (Jiang *et al.*, 2021) (Fig. 6a,b). *MtLBD17/29a* RNAi nodules were smaller than *GUS* RNAi nodules and seemed to lack an active persistent meristem (Fig. 6c,d). In addition, the number of cells within the infection and fixation zones containing living bacteria was dramatically reduced in *MtLBD17/29a* RNAi 1 nodules as compared to *GUS* RNAi nodules as evidenced by live/dead assay using SYTO9/Propidium iodine staining (Fig. 6d). The reduction in nodule number and development caused by *MtLBD17/29a* RNAi negatively impacted root and shoot biomass, reducing the dry weight in 30–45% as compared with *GUS* RNAi plants (Fig. S11). Since nodule occupancy by living bacteria was reduced, we evaluated the density of infection events (number of infection events per root cm), as well as their progression to the cortical cells. The density of infection events was significantly reduced in *MtLBD17/29a* RNAi 1 and *MtLBD17/29a* RNAi 2 as compared with the control *GUS* RNAi roots (Fig. 6e); however, the progression of these infection events was not largely affected by the knockdown of *MtLBD17/29a*. Only the *MtLBD17/29a* RNAi 1 showed a larger proportion of infection events at the microcolony stage as compared to control *GUS* RNAi roots (Fig. 6f). These results indicate that the two genetic programs associated with symbiosis, the nodule organogenesis and the infection by rhizobia, are modulated by *MtLBD17/29a*. Interestingly, overexpression of *MtLBD17/29a* under the CaMV35S promoter also impaired nodule formation (Fig. 6g) and initiation of infection events, but not their progression to the cortical cells (Fig. 6h,i), suggesting that a fine-tune regulation of *MtLBD17/29a* levels is required for the successful establishment of the root nodule symbiosis.

It was previously shown that overexpression of miR390 impaired induction of *MtNSP1* and *MtNSP2* upon rhizobia inoculation (Hobecker *et al.*, 2017). Here, we evaluated whether mRNA levels of these two symbiotic genes, as well as of *MtNF-YA1* and the early nodulin *MtENOD40*, were affected by the knockdown or overexpression of *MtLBD17/29a* (Fig. 7). Induction of both *MtNSP1* and *MtNSP2*, as well as *MtNF-YA1*, in response to *S. meliloti* was diminished in *MtLBD17/29a* silenced roots (Fig. 7). Interestingly, levels of *MtNSP2* were constitutively reduced in *MtLBD17/29a* RNAi roots, that is in uninfected roots. Consistent with the reduction in nodule number and infection events observed in *MtLBD17/29a* overexpressing roots, OXLBD17/29a roots also exhibited reduced rhizobium induced up-regulation of *MtNSP1* and *MtNSP2*. Accumulation of *MtENOD40* mRNAs was not significantly affected by knockdown or overexpression of *MtLBD17/29a* (Fig. 7).

Discussion

Here we identified the class IB member of LBD transcription factors *MtLBD17/29a* as a target of the miR390/*TAS3*/*ARFs* module. Phenotypic characterization upon knockdown and overexpression of *MtLBD17/29a* revealed that this member of the LBD family promotes the elongation of both primary and lateral roots but reduces the initiation of lateral roots. This coincides with the phenotype previously observed in *ARF2/3/4* RNAi roots or *arf4* mutants in *M. truncatula* (Kirolinko *et al.*, 2021), supporting the notion that *MtLBD17/29a* and these ARF members

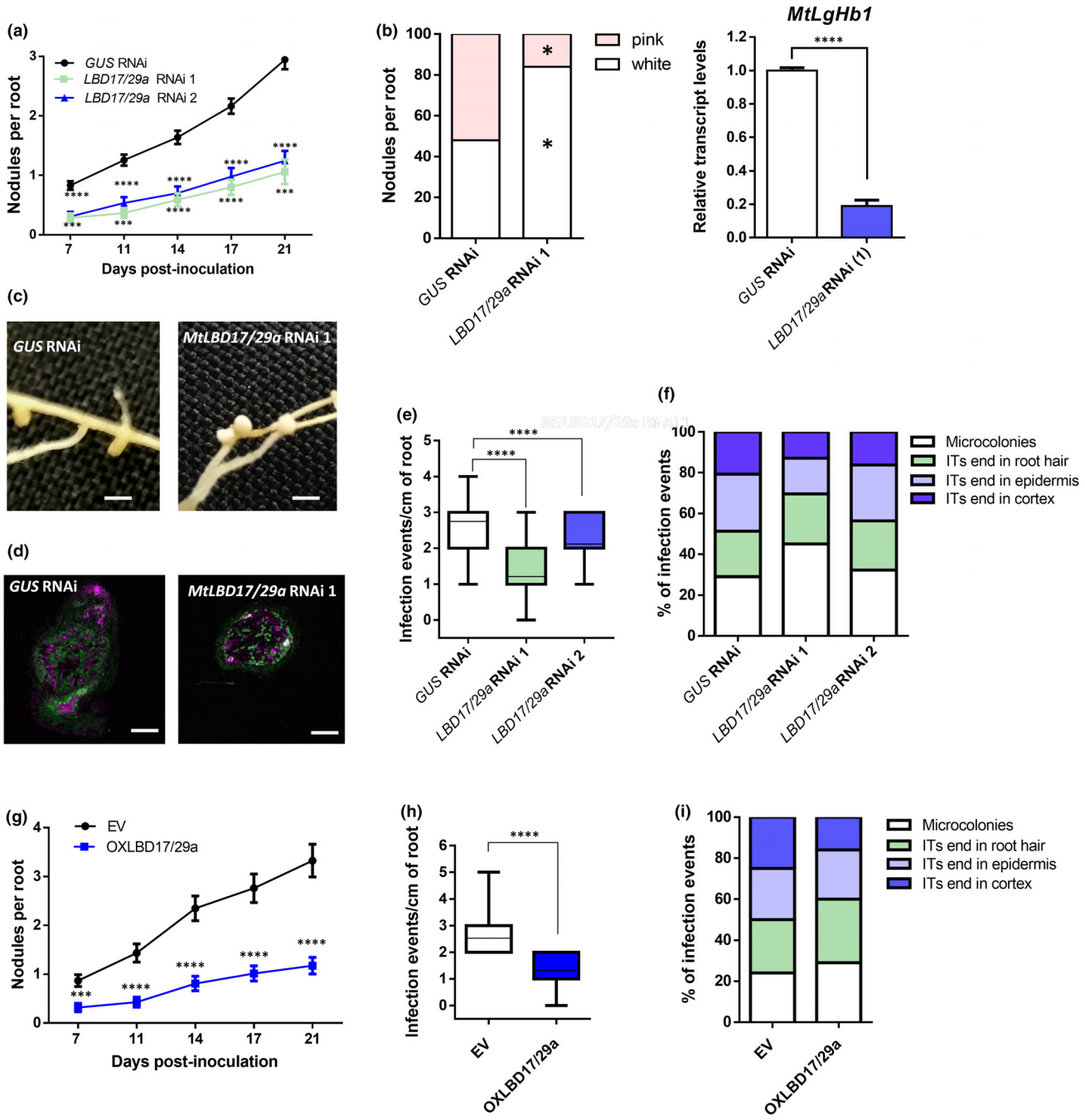

Fig. 6 Knockdown and overexpression of *MtLBD17/29a* affect both nodule development and infection by rhizobia. (a) Time course of nodule formation in *GUS* RNAi, *LBD17/29a* RNAi 1 and *LBD17/29a* RNAi 2 roots upon inoculation with *Sinorhizobium meliloti*. (b) Percentage of pink and white nodules per root (left panel) and relative expression of *MtLgHb1* (right panel) in *GUS* and *LBD17/29a* RNAi 1 roots. (c) Representative picture of nodules formed in *GUS* and *LBD17/29a* RNAi 1 roots. Bars, 0.5 cm. (d) Live/dead bacteria staining of *GUS* and *LBD17/29a* RNAi 1 nodules. Nodules were stained with SYTO9 (green) and propidium iodine (magenta) fluorescent dyes, which reveal cells containing live bacteria and cells with membrane damage, respectively, and visualized by confocal microscopy. Bars, 200 μm. (e) Density of infection events in *GUS* RNAi, *LBD17/29a* RNAi 1 and *LBD17/29a* RNAi 2 at 7 dpi with a *S. meliloti* strain expressing the red fluorescent protein (RFP) protein. (f). Progression of infection events in *GUS* RNAi, *LBD17/29a* RNAi 1 and *LBD17/29a* RNAi 2 roots. (g) Time course of nodule formation in empty vector (EV) and *OXLBD17/29a* roots upon inoculation with *S. meliloti*. (h) Density of infection events in OXLBD17/29a and EV roots 7 dpi with a *S. meliloti* strain expressing the RFP protein. In (a) and (g) error bars represent SE of three independent biological replicates, each with at least 50 roots. In (e) and (h) boxes extend from the 25th to 75th percentiles, the middle line is the median and whiskers extend to the minimum and maximum values of three biological replicates, each with > 25 transgenic roots. Four asterisks indicate statistically significant differences between OXLBD17/29a and EV roots with $P \leq 0.0001$. (i) Progression of infection events in OXLBD17/29a and EV roots. In (f) and (i) infection events were classified as microcolonies, infection threads (ITs) that end in the root hair, in the epidermal cell layer, or reach the cortex at 7 dpi. Each category is presented as the percentage of total infection events. Data are representative of three independent biological replicates, each with > 25 transgenic roots. Asterisks indicate statistically significant differences in an unpaired two-tailed Student's *t*-test (*, $P \leq 0.05$; **, $P \leq 0.01$; ***, $P \leq 0.001$; ****, $P \leq 0.0001$).

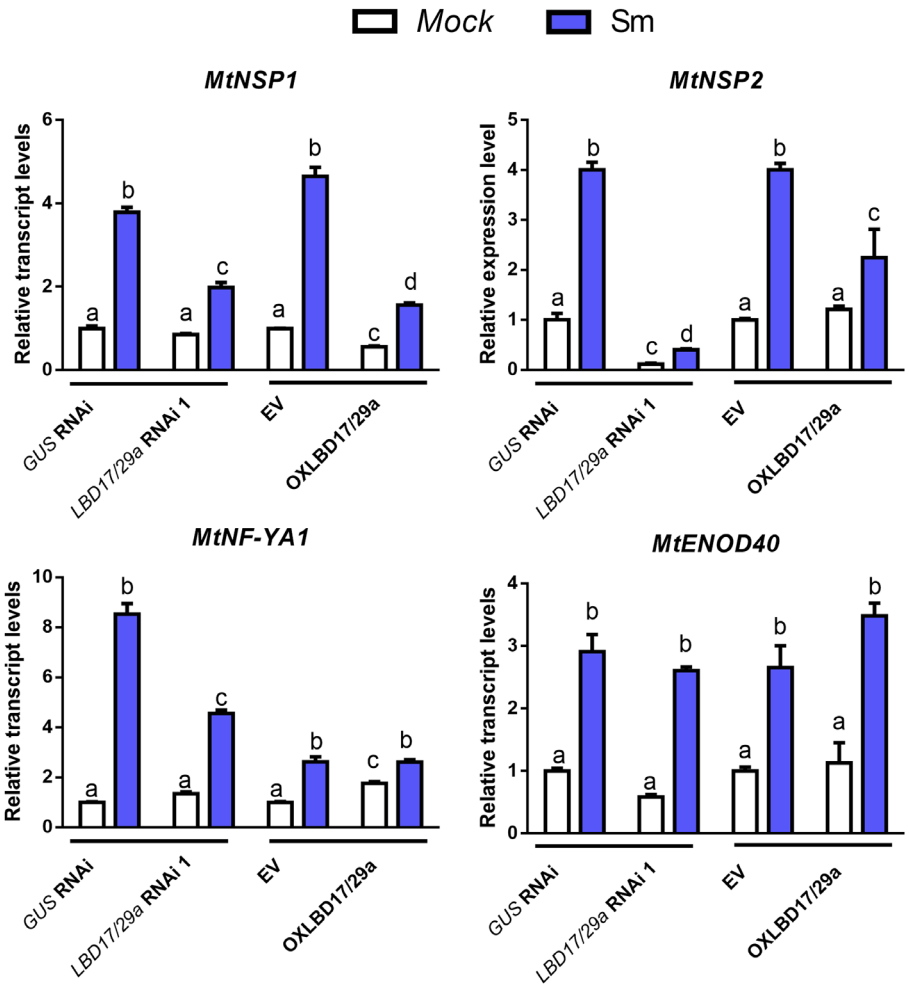

Fig. 7 *MtLBD17/29a* alters induction of *MtNSP1* and *MtNSP2* in response to *Sinorhizobium meliloti*. Transcript levels of early nodulation markers *MtNSP1*, *MtNSP2*, *MtNF-YA1*, and *MtENOD40* in *GUS* RNAi, *LBD17/29a* RNAi 1, empty vector (EV), and OXLBD17/29a roots at 48 h postinoculation (hpi) with *S. meliloti* (Sm, purple bars) or water (mock, white bars) were determined by reverse transcription quantitative polymerase chain reaction, normalized to *MtHIS3L*, and expressed relative to the *GUS* RNAi or EV mock sample. Bars are SEM of three biological replicates. Different letters indicate statistically significant differences between *GUS* RNAi and *LBD17/29a* RNAi 1 or between EV and OXLBD17/29a roots in an unpaired two-tailed Student's *t*-test with $P \leq 0.05$.

are components of the same pathway that contributes to shape the root architecture system. Notably, *MtLBD17/29a* knockdown in *M. truncatula* results in the opposite phenotype to the one exhibited by Arabidopsis *lbd17/29a* double mutants or tomato *sbrl* mutant plants, which exhibited reduced lateral root density (Omary *et al.*, 2022). These observations suggest that ortholog actors may participate in analog pathways across species, albeit inducing distinct developmental outputs, ultimately boosting diversity within the plant kingdom. Distinct outputs in root architecture depending on the species have been previously observed in plants mutated or silenced in auxin response genes such as *ARF2*, *ARF3*, and *ARF4* (Marin *et al.*, 2010; He *et al.*, 2018; Kirolinko *et al.*, 2021) and *ARF16* (Mallory *et al.*, 2005; Bustos-Sanmamed *et al.*, 2013). Species-specific determination mechanisms resulting in variable phenotypes upon mutation of genes involved in auxin signaling and/or response seem to be more extended than anticipated since they have also been observed during leaf development (Yan *et al.*, 2010; Yifhar *et al.*, 2012; Zhou *et al.*, 2013). Such species-specific mechanisms might also result from differences in endogenous auxin levels and/or auxin transport in each species; although we cannot exclude the possibility that the different phenotypes observed in *M. truncatula* as compared to Arabidopsis and tomato are due to the use of an RNAi strategy in this study in contrast to mutant lines in Omary *et al.* (2022).

In the context of root nodule symbiosis, we found that *MtLBD17/29a* was required not only for nodule organogenesis and development, but also for bacterial infection. *MtLBD17/29a* RNAi roots exhibited a reduced number of nodules, which seems to lack a persistent meristem, compared to control *GUS* RNAi nodules. LBD members of the class IB have been shown to regulate the activation of cell cycle genes such as *CYCLINB1,1* and *CYCLIN A1,1-DEPENDENT KINASE* during lateral root formation in Arabidopsis (Lee *et al.*, 2015) or nodule organogenesis in *M. truncatula* (Schiessl *et al.*, 2019). Thus, the phenotype observed in *MtLBD17/29a* RNAi roots could also be attributed to the failure in the activation of the cell cycle genes required to form nodule primordia and the establishment of the nodule meristem. By contrast, nodules formed in roots where the miR390/*TAS3*/*ARF* module has been inactivated by mutations in *AGO7*, which showed enhanced *MtLBD17/29a* mRNA levels, exhibited multiple meristems (Hobecker *et al.*, 2017), reinforcing the notion that *MtLBD17/29a* might act downstream of the miR390/TAS3/ARF module controlling meristem

formation. The observation that most of the nodules formed in *MtLBD17/29a* RNAi roots were white and the dramatic reduction in the expression levels of the leghemoglobin coding gene *MtLhGb1* suggest that nodules formed *MtLBD17/29a* RNAi roots are nonfunctional in nitrogen fixation. Moreover, *MtLBD17/29a* RNAi nodules exhibited a limited number of cells containing living bacteria, which might be a consequence of the altered bacterial colonization through infection threads. This infection mechanism requires extensive cell wall remodeling to allow the formation of infection pockets and the elongation of ITs (Su *et al.*, 2023). It has been reported that members of the LBD class IB modulate the expression of genes encoding cell wall remodeling enzymes. AtLBD18 was shown to modulate the expression of *EXPANSIN14*, *EXPANSIN17*, and *POLYGALACTURONASE* upon an increase in auxin concentration, facilitating the emergence of lateral roots through softening and remodeling of the cell wall (Lee *et al.*, 2013). In addition, *lbd29-1* mutant roots failed to induce *POLYGALACTURONASE* expression following auxin treatment (Porco *et al.*, 2016). In this context, the decrease in the density of infection events observed in *MtLBD17/29a* silenced roots might be related to defects in the cell wall remodeling required to initiate bacterial infection events through root hairs.

The reduced nodulation and infection phenotype observed in *MtLBD17/29a* overexpressing roots may be due to its ectopic expression, which could alter the expression of nodulation regulatory genes in tissues other than those normally expressing *MtLBD17/29a*. Alternatively, MtLBD17/29a could form transcriptional complexes with additional components. Both the increase and the reduction of *MtLBD17/29a* levels would alter the stoichiometry of the components, resulting in nonfunctional transcriptional complexes. This hypothesis is supported by previous findings demonstrating that LBD members could form homodimers (Lee *et al.*, 2017) or interact with other transcription factors, such as members of the ARF family, to cooperatively promote transcriptional activation of their target genes (Pandey *et al.*, 2018).

Reverse transcription quantitative polymerase chain reaction experiments showed that *MtLBD17/29a* expression is dependent on *MtARF2*, *MtARF3* and *MtARF4a/b*, whereas ChIP-PCR experiments indicated that MtARF2 binds with high affinity to the *MtLBD17/29a* promoter region activating its expression. However, it should be considered that other ARF members or additional transcription factors might also modulate the expression of *MtLBD17/29a*. The nodulation and infection phenotype of *MtLBD17/29a* RNAi roots is reminiscent of that observed in miR390 overexpressing roots (Hobecker *et al.*, 2017), in roots silenced in *MtARF2*, *MtARF3*, and *MtARF4a/b* or in the *arf4a* mutant (Kirolinko *et al.*, 2021). The expression pattern of *MtLBD17/29a* promoter coincides with that previously described for *MtARF4a* in the infection, transition, and nitrogen fixation zones of nodules (Kirolinko *et al.*, 2021) and partially overlaps with the previously described *MtARF2* mRNA expression pattern previously observed in the nodule differentiation zones (Hobecker *et al.*, 2017). It should be noted that the promoter of *MIR390b* is active in the nodule meristem and mRNA levels of *MtTAS3* and *MtAGO7* accumulated at higher levels in the nodule meristem (Hobecker *et al.*, 2017). Thus, it can be speculated that the miR390/*TAS3*-mediated production of tasiARFs might posttranscriptionally repress ARF transcripts in the nodule meristematic zone and consequently, restrict the expression of *MtLBD17/29a* to nonmeristematic zones of the nodule. Altogether, these data suggest a hierarchical activation of ARFs and LBD transcription factors that positively modulate the root nodule symbiosis. Hierarchical activation of ARFs and LBD transcription factors was previously observed in Arabidopsis, where AtARF7 and AtARF19 promote transcriptional activation of *AtLBD16*, *AtLBD18*, *AtLBD29*, and *AtLBD33* in response to auxin during lateral root development (Okushima *et al.*, 2007). This suggests that ARF-mediated transcriptional activation of LBDs might be a common regulatory mechanism that mediates the formation of lateral root organs. Full activation of *MtLBD17/29a* in response to Nod Factor or rhizobia also requires the master regulator *MtNIN*, but not *MtNF-YA1*, which was shown to be required for activation of *MtARF2*, *MtARF3*, and *MtARF4* (Kirolinko *et al.*, 2021). Transcriptional activation of *MtNF-YA1* also depends on *NIN* (Soyano *et al.*, 2013), and our analysis of early nodulation markers indicated that full activation of *MtNF-YA1* in response to rhizobia also requires *MtLBD17/29a*. This suggests an intricated regulatory mechanism involving hierarchical transcriptional activation and positive feedback loops controlling the expression of these transcription factors. *MtNIN* was also required for the activation of *LBD16* in response to rhizobia (Schiessl *et al.*, 2019; Soyano *et al.*, 2021). Both *LBD16* and *LBD17/29a* have been implicated in the control of lateral root development in different plant species (Okushima *et al.*, 2007; Omary *et al.*, 2022) and the organogenesis of symbiotic nodule in legumes (Schiessl *et al.*, 2019; Soyano *et al.*, 2019, and this work). This suggests that both LBD members might be part of a key regulatory mechanism operating in lateral root development that was co-opted by legumes to coordinate nodule organogenesis. Although both *MtLBD16* and *MtLBD17/29*a are NIN-dependent, their expression pattern does not fully overlap upon *S. meliloti* infection based on spot inoculation RNA-Seq data (Schiessl *et al.*, 2019). In addition, they seem to modulate the expression of different early nodulation genes, for example MtLBD17/29a, but not MtLBD16, mediates activation of *MtNF-YA1* and *MtNSP1* whereas MtLBD16 instead activates *MtNFP* and *MtNF-YB18* (Schiessl *et al.*, 2019). Furthermore, alteration of *MtLBD17/29a* levels impaired not only nodule development but also bacterial infection.

Activation of *MtNSP1* and *MtNSP2* in response to rhizobia requires fine-tuned regulation of *MtLBD17/29*a levels since both overexpression and silencing of *MtLBD17/29a* partially impaired the induction of these early symbiotic genes. *MtNSP2* also requires the *MtARF2*, *MtARF3*, and *MtARF4a* members for its activation in response to rhizobia (Kirolinko *et al.*, 2021). Moreover, *MtNSP2* is a direct target of MtARF2. An inspection of the *MtNSP2* promoter revealed that, in addition to the two ARE motifs, it contains three LBD binding sites, supporting the notion that both MtLBD17/29a and MtARF2 may act cooperatively to activate the transcription of *MtNSP2* at early stages of

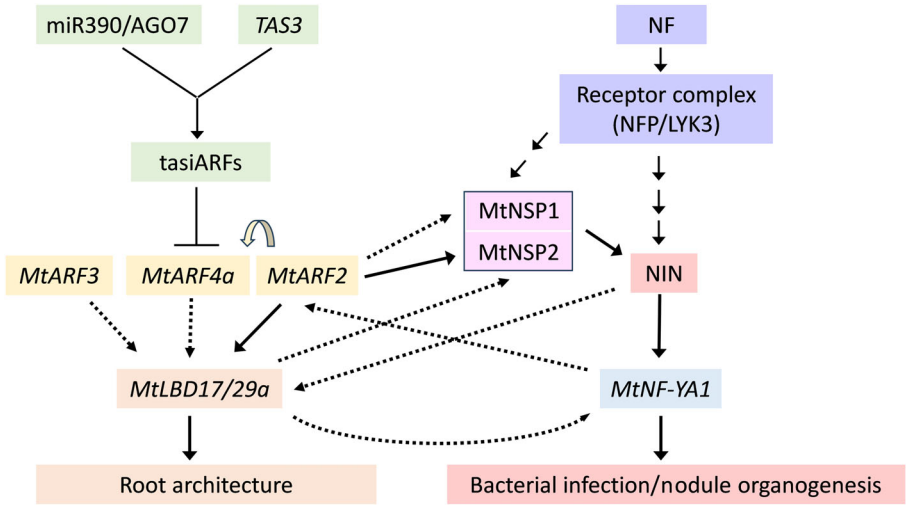

Fig. 8 Integrated model proposing a crosstalk between the miR390/TAS3/ARF module with MtLBD17/29 and the Nod signaling pathway. Endonucleolytic cleavage of *TAS3* by the miR390-guided AGO7 leads to the production of tasiARFs, which subsequently posttranscriptionally repress *MtARF2*, *MtARF3* and *MtARF4*. MtARF2 plays a role in targeting and activating the expression of *MtLBD17/29a* but also directly binds the *MtARF4a* promoter providing a possible positive feedback loop. MtARFs and MtLBD17/29a control root architecture by promoting lateral root elongation and limiting lateral root formation. In addition, MtARF2 directly targets the promoter of the early nodulation marker *MtNSP2*, intersecting the Nod signaling pathway. *MtLBD17/29a* is also required for induction in response to rhizobia of *MtNSP1* and *MtNF-YA1*, two genes required for both bacterial infection and nodule organogenesis. In addition, activation of *MtLBD17/29a* in response to Nod Factor (NF) or rhizobia is NIN-dependent, revealing an additional link between MtLBD17/29a and the Nod signaling pathway. Solid arrows represent direct interaction, whereas dashed arrows indicate direct or indirect interaction between components. Blunt ended arrow indicates posttranscriptional repression of gene expression.

the root nodule symbiosis. Thus, activation of *MtARF2* mediated by inactivation of the miR390/*TAS3* module, could promote direct activation of both *MtLBD17/29a* and *MtNSP2*, and in turn *MtLBD17/29* might further promote directly or indirectly activation of *MtNSP2* in response to rhizobia. Based on previous results and those presented here, we propose an integrated model that links the pathway involving the miR390/*TAS3/ARFs* module along with *MtLBD17/29a* in the control of root architecture and its intersection with the Nod Factor signaling pathway in *M. truncatula* (Fig. 8). The transcription factor MtNF-YA1 is required for induction of *MtARF2*, *MtARF3* and *MtARF4a* in response to rhizobia (Kirolinko *et al.*, 2021), whereas the miR390/*TAS3* module is inactivated at early stages of the symbiosis releasing posttranscriptional repression of *MtARF2*, *MtARF3* and *MtARF4a* (Hobecker *et al.*, 2017). Downstream of this module, MtARF2 binds to the *MtLBD17/29a* promoter activating its expression. Interestingly, MtARF2 also binds to the *MtARF4a* promoter, which might represent a positive feedback loop to promote the elongation of primary and secondary roots. In addition, MtARF2 binds to the *MtNSP2* promoter, intersecting the nodulation signaling pathway. *MtLBD17/29a* is also directly or indirectly regulated by *MtNIN* and, in turn, modulates the expression of *MtNSP1*, *MtNSP2*, and *MtNF-YA1*, promoting the formation of nitrogen-fixing nodules.

Finally, the ectopic expression of *MtLBD17/29a* was sufficient to inhibit lateral root initiation and promote lateral root elongation; however, it was not sufficient to promote nodule organogenesis and bacterial infection. Instead, ectopic expression of *MtLBD17/29a* disrupts transcriptional activation of essential symbiotic genes such as *MtNSP1* and *MtNSP2* resulting in reduced density of infection events and nodule number. These results indicate that additional regulatory components should be required to completely fill the function of *MtLBD17/29a* during the formation of nitrogen-fixing nodules. The identification of such additional regulatory components will shed light on the distinct playing roles of *MtLBD17/29a* that underly lateral root and nodule development.

Acknowledgements

We would like to thank Mauricio Reynoso for critical reading and Julia Bailey-Serres for fruitful discussions. This work was financially supported by grants of the Agencia Nacional de Promoción de la Investigación, el Desarrollo Tecnológico y la Innovaciónn (Agencia I+D+I) of Argentina, FONCYT (PICT2019-00554 and PICT2020-00053), the Ministerio de Ciencia, Tecnología e Innovación (MINCyT) of Argentina (RIBOLEG, CONVE-2023-100766842) and by the International Research Project LOCOSYM of the CNRS. FA, FAB and MEZ are members of CONICET. CK and MC are funded by CONICET fellowships.

Competing interests

None declared.

Author contributions

CK, MC, FA, KH, AC and AN conducted the experiments; FAB, FA, MC and MEZ designed research; CK, FAB and MEZ analyzed data; CK, FAB and MEZ wrote the paper.

ORCID

Federico Ariel https://orcid.org/0000-0001-8478-8808
Flavio Antonio Blanco https://orcid.org/0000-0002-8380-8472
Aurélie Christ https://orcid.org/0000-0003-1946-1926
Martín Crespi https://orcid.org/0000-0002-5698-9482
Andreas Niebel https://orcid.org/0000-0002-3402-8381
María Eugenia Zanetti https://orcid.org/0000-0001-9565-1743

Data availability

Sequence information of protein-coding genes used in this study was obtained from the *M. truncatula* genome MtrunA17r5.0-ANR under the following accession nos.: *MtLBD17/29a* (MtrunA17_Chr1g0184271), *MtLBD17/29b* (MtrunA17_Chr7g0261031), *MtARF2* (MtrunA17_Chr8g0385791), *MtARF3* (MtrunA17_Chr2g0282961), *MtARF4a* (MtrunA17_Chr4g0029671), *MtARF4b* (MtrunA17_Chr2g0326281), *MtNSP1* (MtrunA17_Chr8g0344101), *MtNSP2* (MtrunA17_Chr3g0114841), *MtNIN* (MtrunA17_Chr5g0448621), *MtERN1* (MtrunA17_Chr7g0253424), *MtNF-YA1* (MtrunA17_Chr1g0148951) and *MtENOD40* (MtrunA17_Chr8g0368441). Raw RNA-Seq data are available from Gene Expression Omnibus database in NCBI (www.ncbi.nlm.nih.gov/) under the accession GSE248872 (https://www.ncbi.nlm.nih.gov/geo/query/acc.cgi?acc=GSE248872).

References

Ariel F, Diet A, Verdenaud M, Gruber V, Frugier F, Chan R, Crespi M. 2010. Environmental regulation of lateral root emergence in *Medicago truncatula* requires the HD-Zip I transcription factor HB1. *Plant Cell* **22**: 2171–2183.

Ariel F, Lucero L, Christ A, Mammarella MF, Jegu T, Veluchamy A, Mariappan K, Latrasse D, Blein T, Liu C *et al.* 2020. R-loop mediated trans action of the APOLO long noncoding RNA. *Molecular Cell* 77: 1055–1065.

Ariel FD, Diet A, Crespi M, Chan RL. 2010. The LOB-like transcription factor Mt LBD1 controls *Medicago truncatula* root architecture under salt stress. *Plant Signaling & Behavior* **5**: 1666–1668.

Bishopp A, Bennett MJ. 2019. Turning lateral roots into nodules. *Science* **366**: 953–954.

Boisson-Dernier A, Chabaud M, Garcia F, Becard G, Rosenberg C, Barker DG. 2001. *Agrobacterium rhizogenes*-transformed roots of *Medicago truncatula* for the study of nitrogen-fixing and endomycorrhizal symbiotic associations. *Molecular Plant–Microbe Interactions* **14**: 695–700.

Breakspear A, Liu C, Roy S, Stacey N, Rogers C, Trick M, Morieri G, Mysore KS, Wen J, Oldroyd GE *et al.* 2014. The root hair "infectome" of *Medicago truncatula* uncovers changes in cell cycle genes and reveals a requirement for auxin signaling in rhizobial infection. *Plant Cell* **26**: 4680–4701.

Bustos-Sanmamed P, Mao G, Deng Y, Elouet M, Khan GA, Bazin J, Turner M, Subramanian S, Yu O, Crespi M *et al.* 2013. Overexpression of miR160 affects root growth and nitrogen-fixing nodule number in *Medicago truncatula*. *Functional Plant Biology* **40**: 1208–1220.

Cabrera J, Diaz-Manzano FE, Sanchez M, Rosso MN, Melillo T, Goh T, Fukaki H, Cabello S, Hofmann J, Fenoll C *et al.* 2014. A role for LATERAL ORGAN BOUNDARIES-DOMAIN 16 during the interaction *Arabidopsis-Meloidogyne* spp. provides a molecular link between lateral root and root-knot nematode feeding site development. *New Phytologist* **203**: 632–645.

Castaingts M, Kirolinko C, Rivero C, Artunian J, Mancini Villagra U, Blanco FA, Zanetti ME. 2022. Identification of conserved and new miRNAs that affect nodulation and strain selectivity in the *Phaseolus vulgaris-Rhizobium etli* symbiosis through differential analysis of host small RNAs. *New Phytologist* **234**: 1430–1447.

Cervantes-Perez SA, Thibivilliers S, Laffont C, Farmer AD, Frugier F, Libault M. 2022. Cell-specific pathways recruited for symbiotic nodulation in the *Medicago truncatula* legume. *Molecular Plant* **15**: 1868–1888.

Dang TVT, Lee S, Cho H, Choi K, Hwang I. 2023. The LBD11-ROS feedback regulatory loop modulates vascular cambium proliferation and secondary growth in Arabidopsis. *Molecular Plant* **16**: 1131–1145.

Fahraeus G. 1957. The infection of clover root hairs by nodule bacteria studied by a simple glass slide technique. *Journal of General Microbiology* **16**: 374–381.

Fan M, Xu C, Xu K, Hu Y. 2012. LATERAL ORGAN BOUNDARIES DOMAIN transcription factors direct callus formation in Arabidopsis regeneration. *Cell Research* **22**: 1169–1180.

Guo M, Thomas J, Collins G, Timmermans MCP. 2008. Direct repression of KNOX loci by the ASYMMETRIC LEAVES1 complex of Arabidopsis. *Plant Cell* **20**: 48–58.

He F, Xu C, Fu X, Shen Y, Guo L, Leng M, Luo K. 2018. The microRNA390/TRANS-ACTING SHORT INTERFERING RNA3 module mediates lateral root growth under salt stress via the auxin pathway. *Plant Physiology* **177**: 775–791.

Hobecker KV, Reynoso MA, Bustos-Sanmamed P, Wen J, Mysore KS, Crespi M, Blanco FA, Zanetti ME. 2017. The microRNA390/TAS3 pathway mediates symbiotic nodulation and lateral root growth. *Plant Physiology* **174**: 2469–2486.

Hu Y, Zhang J, Jia H, Sosso D, Li T, Frommer WB, Yang B, White FF, Wang N, Jones JB. 2014. Lateral organ boundaries 1 is a disease susceptibility gene for citrus bacterial canker disease. *Proceedings of the National Academy of Sciences, USA* **111**: E521–E529.

Jhu M-Y, Oldroyd GED. 2023. Dancing to a different tune, can we switch from chemical to biological nitrogen fixation for sustainable food security? *PLoS Biology* **21**: e3001982.

Jiang S, Jardinaud MF, Gao J, Pecrix Y, Wen J, Mysore K, Xu P, Sanchez-Canizares C, Ruan Y, Li Q *et al.* 2021. NIN-like protein transcription factors regulate leghemoglobin genes in legume nodules. *Science* **374**: 625–628.

Karimi M, Depicker A, Hilson P. 2007. Recombinational cloning with plant gateway vectors. *Plant Physiology* **145**: 1144–1154.

Karimi M, Inze D, Depicker A. 2002. GATEWAY vectors for *Agrobacterium*-mediated plant transformation. *Trends in Plant Science* **7**: 193–195.

Kim D, Paggi JM, Park C, Bennett C, Salzberg SL. 2019. Graph-based genome alignment and genotyping with HISAT2 and HISAT-GENOTYPE. *Nature Biotechnology* **37**: 907–915.

Kim MJ, Kim M, Lee MR, Park SK, Kim J. 2015. LATERAL ORGAN BOUNDARIES DOMAIN (LBD)10 interacts with SIDECAR POLLEN/LBD27 to control pollen development in Arabidopsis. *The Plant Journal* **81**: 794–809.

Kirolinko C, Hobecker K, Wen J, Mysore KS, Niebel A, Blanco FA, Zanetti ME. 2021. Auxin response factor 2 (ARF2), ARF3, and ARF4 mediate both lateral root and nitrogen fixing nodule development in *Medicago truncatula*. *Frontiers in Plant Science* **12**: 659061.

Laporte P, Lepage A, Fournier J, Catrice O, Moreau S, Jardinaud MF, Mun JH, Larrainzar E, Cook DR, Gamas P *et al.* 2014. The CCAAT box-binding transcription factor NF-YA1 controls rhizobial infection. *Journal of Experimental Botany* **65**: 481–494.

Lee HW, Cho C, Kim J. 2015. Lateral organ boundaries domain16 and 18 act downstream of the AUXIN1 and LIKE-AUXIN3 auxin influx carriers to

control lateral root development in Arabidopsis. *Plant Physiology* **168**: 1792–1806.

Lee HW, Kang NY, Pandey SK, Cho C, Lee SH, Kim J. 2017. Dimerization in LBD16 and LBD18 transcription factors is critical for lateral root formation. *Plant Physiology* **174**: 301–311.

Lee HW, Kim MJ, Kim NY, Lee SH, Kim J. 2013. LBD18 acts as a transcriptional activator that directly binds to the EXPANSIN14 promoter in promoting lateral root emergence of Arabidopsis. *The Plant Journal* **73**: 212–224.

Lee HW, Kim NY, Lee DJ, Kim J. 2009. LBD18/ASL20 regulates lateral root formation in combination with LBD16/ASL18 downstream of ARF7 and ARF19 in Arabidopsis. *Plant Physiology* **151**: 1377–1389.

Love MI, Huber W, Anders S. 2014. Moderated estimation of fold change and dispersion for RNA-seq data with DESeq2. *Genome Biology* **15**: 550.

Majer C, Hochholdinger F. 2011. Defining the boundaries: structure and function of LOB domain proteins. *Trends in Plant Science* **16**: 47–52.

Mallory AC, Bartel DP, Bartel B. 2005. MicroRNA-directed regulation of Arabidopsis AUXIN RESPONSE FACTOR17 is essential for proper development and modulates expression of early auxin response genes. *Plant Cell* **17**: 1360–1375.

Mangeon A, Bell EM, Lin WC, Jablonska B, Springer PS. 2011. Misregulation of the LOB domain gene DDA1 suggests possible functions in auxin signalling and photomorphogenesis. *Journal of Experimental Botany* **62**: 221–233.

Marin E, Jouannet V, Herz A, Lokerse AS, Weijers D, Vaucheret H, Nussaume L, Crespi MD, Maizel A. 2010. miR390, Arabidopsis TAS3 tasiRNAs, and their AUXIN RESPONSE FACTOR targets define an autoregulatory network quantitatively regulating lateral root growth. *Plant Cell* **22**: 1104–1117.

Marsh JF, Rakocevic A, Mitra RM, Brocard L, Sun J, Eschstruth A, Long SR, Schultze M, Ratet P, Oldroyd GE. 2007. *Medicago truncatula* NIN is essential for rhizobial-independent nodule organogenesis induced by autoactive calcium/calmodulin-dependent protein kinase. *Plant Physiology* **144**: 324–335.

Meade HM, Signer ER. 1977. Genetic mapping of *Rhizobium meliloti*. *Proceedings of the National Academy of Sciences, USA* **74**: 2076–2078.

Middleton PH, Jakab J, Penmetsa RV, Starker CG, Doll J, Kalo P, Prabhu R, Marsh JF, Mitra RM, Kereszt A *et al.* 2007. An ERF transcription factor in *Medicago truncatula* that is essential for Nod factor signal transduction. *Plant Cell* **19**: 1221–1234.

Moreno-Risueno MA, Van Norman JM, Moreno A, Zhang J, Ahnert SE, Benfey PN. 2010. Oscillating gene expression determines competence for periodic *Arabidopsis* root branching. *Science* **329**: 1306–1311.

Mustroph A, Lee SC, Oosumi T, Zanetti ME, Yang H, Ma K, Yaghoubi-Masihi A, Fukao T, Bailey-Serres J. 2010. Cross-kingdom comparison of transcriptomic adjustments to low-oxygen stress highlights conserved and plant-specific responses. *Plant Physiology* **152**: 1484–1500.

Ng JLP, Hassan S, Truong TT, Hocart CH, Laffont C, Frugier F, Mathesius U. 2015. Flavonoids and auxin transport inhibitors rescue symbiotic nodulation in the *Medicago truncatula* cytokinin perception mutant cre1. *Plant Cell* **27**: 2210–2226.

Oh SA, Park KS, Twell D, Park SK. 2010. The SIDECAR POLLEN gene encodes a microspore-specific LOB/AS2 domain protein required for the correct timing and orientation of asymmetric cell division. *The Plant Journal* **64**: 839–850.

Okushima Y, Fukaki H, Onoda M, Theologis A, Tasaka M. 2007. ARF7 and ARF19 regulate lateral root formation via direct activation of LBD/ASL genes in Arabidopsis. *Plant Cell* **19**: 118–130.

Omary M, Gil-Yarom N, Yahav C, Steiner E, Hendelman A, Efroni I. 2022. A conserved superlocus regulates above- and belowground root initiation. *Science* **375**: eabf4368.

Pandey SK, Lee HW, Kim MJ, Cho C, Oh E, Kim J. 2018. LBD18 uses a dual mode of a positive feedback loop to regulate ARF expression and transcriptional activity in Arabidopsis. *The Plant Journal* **95**: 233–251.

Pecrix Y, Staton SE, Sallet E, Lelandais-Briere C, Moreau S, Carrere S, Blein T, Jardinaud MF, Latrasse D, Zouine M *et al.* 2018. Whole-genome landscape of *Medicago truncatula* symbiotic genes. *Nature Plants* **4**: 1017–1025.

Pertea M, Pertea GM, Antonescu CM, Chang TC, Mendell JT, Salzberg SL. 2015. StringTie enables improved reconstruction of a transcriptome from RNA-seq reads. *Nature Biotechnology* **33**: 290–295.

Porco S, Larrieu A, Du Y, Gaudinier A, Goh T, Swarup K, Swarup R, Kuempers B, Bishopp A, Lavenus J *et al.* 2016. Lateral root emergence in Arabidopsis is dependent on transcription factor LBD29 regulation of auxin influx carrier LAX3. *Development* **143**: 3340–3349.

Quandt HJ, Pühler A, Broer I. 1993. Transgenic root nodules of *Vicia hirsuta*: a fast and efficient system for the study of gene expression in indeterminate-type nodules. *Molecular Plant–Microbe Interactions* **6**: 699–706.

Reynoso MA, Blanco FA, Bailey-Serres J, Crespi M, Zanetti ME. 2013. Selective recruitment of mRNAs and miRNAs to polyribosomes in response to rhizobia infection in *Medicago truncatula*. *The Plant Journal* **73**: 289–301.

Roux B, Rodde N, Jardinaud M, Timmers T, Sauviac L, Cottret L, Carrère S, Sallet E, Courcelle E, Moreau S *et al.* 2014. An integrated analysis of plant and bacterial gene expression in symbiotic root nodules using laser-capture microdissection coupled to RNA sequencing. *The Plant Journal* **77**: 817–837.

Roy S, Liu W, Nandety RS, Crook A, Mysore KS, Pislariu CI, Frugoli J, Dickstein R, Udvardi MK. 2020. Celebrating 20 years of genetic discoveries in legume nodulation and symbiotic nitrogen fixation. *Plant Cell* **32**: 15–41.

Schiessl K, Lilley JLS, Lee T, Tamvakis I, Kohlen W, Bailey PC, Thomas A, Luptak J, Ramakrishnan K, Carpenter MD *et al.* 2019. NODULE INCEPTION recruits the lateral root developmental program for symbiotic nodule organogenesis in *Medicago truncatula*. *Current Biology* **29**: 3657–3668.

Shuai B, Reynaga-Peña CG, Springer PS. 2002. The lateral organ boundaries gene defines a novel, plant-specific gene family. *Plant Physiology* **129**: 747–761.

Soyano T, Kouchi H, Hirota A, Hayashi M. 2013. Nodule inception directly targets NF-Y subunit genes to regulate essential processes of root nodule development in *Lotus japonicus*. *PLoS Genetics* **9**: e1003352.

Soyano T, Liu M, Kawaguchi M, Hayashi M. 2021. Leguminous nodule symbiosis involves recruitment of factors contributing to lateral root development. *Current Opinion in Plant Biology* **59**: 102000.

Soyano T, Shimoda Y, Kawaguchi M, Hayashi M. 2019. A shared gene drives lateral root development and root nodule symbiosis pathways in *Lotus*. *Science* **366**: 1021–1023.

Su C, Zhang G, Rodriguez-Franco M, Hinnenberg R, Wietschorke J, Liang P, Yang W, Uhler L, Li X, Ott T. 2023. Transcellular progression of infection threads in *Medicago truncatula* roots is associated with locally confined cell wall modifications. *Current Biology* **33**: 533–542.

Thatcher LF, Powell JJ, Aitken EA, Kazan K, Manners JM. 2012. The lateral organ boundaries domain transcription factor LBD20 functions in *Fusarium* wilt susceptibility and jasmonate signaling in Arabidopsis. *Plant Physiology* **160**: 407–418.

Tian CF, Garnerone AM, Mathieu-Demaziere C, Masson-Boivin C, Batut J. 2012. Plant-activated bacterial receptor adenylate cyclases modulate epidermal infection in the *Sinorhizobium meliloti-Medicago* symbiosis. *Proceedings of the National Academy of Sciences, USA* **109**: 6751–6756.

Traubenik S, Reynoso MA, Hobecker K, Lancia M, Hummel M, Rosen B, Town C, Bailey-Serres J, Blanco F, Zanetti ME. 2020. Reprogramming of root cells during nitrogen-fixing symbiosis involves dynamic polysome association of coding and noncoding RNAs. *Plant Cell* **32**: 352–373.

Vandesompele J, De Preter K, Pattyn F, Poppe B, Van Roy N, De Paepe A, Speleman F. 2002. Accurate normalization of real-time quantitative RT-PCR data by geometric averaging of multiple internal control genes. *Genome Biology* **3**: research0034.

Xia R, Xu J, Meyers BC. 2017. The emergence, evolution, and diversification of the miR390-TAS3-ARF pathway in land plants. *Plant Cell* **29**: 1232–1247.

Xiao TT, Schilderink S, Moling S, Deinum EE, Kondorosi E, Franssen H, Kulikova O, Niebel A, Bisseling T. 2014. Fate map of *Medicago truncatula* root nodules. *Development* **141**: 3517–3528.

Xu C, Luo F, Hochholdinger F. 2016. LOB domain proteins: beyond lateral organ boundaries. *Trends in Plant Science* **21**: 159–167.

Yan J, Cai X, Luo J, Sato S, Jiang Q, Yang J, Cao X, Hu X, Tabata S, Gresshoff PM *et al.* 2010. The REDUCED LEAFLET genes encode key components of the trans-acting small interfering RNA pathway and regulate compound leaf and flower development in *Lotus japonicus*. *Plant Physiology* **152**: 797–807.

Yifhar T, Pekker I, Peled D, Friedlander G, Pistunov A, Sabban M, Wachsman G, Alvarez JP, Amsellem Z, Eshed Y. 2012. Failure of the tomato trans-acting short interfering RNA program to regulate AUXIN RESPONSE FACTOR3 and ARF4 underlies the wiry leaf syndrome. *Plant Cell* **24**: 3575–3589.

Zhang Y, Li Z, Ma B, Hou Q, Wan X. 2020. Phylogeny and functions of LOB domain proteins in plants. *International Journal of Molecular Sciences* **21**: 2278.

Zhou C, Han L, Fu C, Wen J, Cheng X, Nakashima J, Ma J, Tang Y, Tan Y, Tadege M *et al.* 2013. The trans-acting short interfering RNA3

pathway and no apical meristem antagonistically regulate leaf margin development and lateral organ separation, as revealed by analysis of an argonaute7/lobed leaflet1 mutant in *Medicago truncatula*. *Plant Cell* **25**: 4845–4862.

Supporting Information

Additional Supporting Information may be found online in the Supporting Information section at the end of the article.

Fig. S1 Reproducibility between biological replicates.

Fig. S2 Gene Ontology classification of DEGs in EV and OX390 roots in response to *Sinorhizobium meliloti*.

Fig. S3 Phylogenetic tree analysis of the LBD family genes in *Arabidopsis thaliana* and *Medicago truncatula*.

Fig. S4 Synteny between the gene *MtrunA17Chr1g0184271* (*Medtr1g070205*) and *AtLBD17* (A) and *AtLBD29* (B).

Fig. S5 Phenotypic analysis of *MtARF2* overexpressing roots.

Fig. S6 Expression of the class IB members of the LBD family during lateral root formation in *Medicago truncatula*.

Fig. S7 Root architecture phenotype in *MtLBD17/29a* RNAi in the presence of nitrogen.

Fig. S8 Root architecture phenotype in *MtLBD17/29a* overexpressing roots.

Fig. S9 Expression analysis of the class IB LBD members in *Medicago truncatula* during root nodule symbiosis.

Fig. S10 Expression of *MtARF2* in roots cells.

Fig. S11 Shoot and root biomass of *GUS* RNAi and *MtLBD17/29a* RNAi plants.

Table S1 Primers used in this study.

Table S2 Total and mapped reads.

Table S3 Fold change of all gene in EV and OX390 roots at 48 hpi postinoculation.

Table S4 DEGs upregulated in EV roots at 48 hpi postinoculation.

Table S5 DEGs downregulated in EV roots at 48 hpi postinoculation.

Table S6 DEGs upregulated in OX390 roots at 48 hpi postinoculation.

Table S7 DEGs downregulated in OX390 roots at 48 hpi postinoculation.

Table S8 Nodulation markers in EV and OX390 at 48 hpi with *Sinorhizobium meliloti* vs mock.

Table S9 DEGs encoding transcription factors.

Please note: Wiley is not responsible for the content or functionality of any Supporting Information supplied by the authors. Any queries (other than missing material) should be directed to the *New Phytologist* Central Office.